Complete angular analysis of polarized top quark decay at $O(\alpha_s)$

M. Fischer, S. Groote, J. G. Körner, and M. C. Mauser
Institut für Physik, Johannes-Gutenberg-Universität, Staudinger Weg 7, D-55099 Mainz, Germany
(Received 31 January 2001; published 20 February 2002)

We calculate the full $O(\alpha_s)$ radiative corrections to the three spin independent and five spin dependent structure functions that describe the angular decay distribution in the decay of a polarized top quark into a W boson (followed by the decay $W^+ \to l^+ + \nu_l$ or by $W^+ \to \bar{q} + q$) and a bottom quark. The angular decay distribution is described in cascade fashion; i.e., the decay $t(\uparrow) \to W^+ + X_b$ is analyzed in the top-quark rest system while the subsequent decay $W^+ \to l^+ + \nu_l$ (or $W^+ \to \bar{q} + q$) is analyzed in the W rest frame. Since the structure function ratios depend on the ratio m_W/m_t we advocate the use of such angular decay measurements for the determination of the top quark's mass. Our results for the eight $O(\alpha_s)$ integrated structure functions are presented in analytical form, keeping the mass of the bottom quark finite. In the limit $m_b \to 0$ the structure function expressions reduce to rather compact forms. We also present results for the $m_b = 0$ unpolarized and polarized $O(\alpha_s)$ scalar structure functions relevant to the semi-inclusive decay of a polarized top quark into a charged Higgs boson $t(\uparrow) \to H^+ + X_b$ in the two-Higgs-doublet model when $m_b = 0$.

DOI: 10.1103/PhysRevD.65.054036 PACS number(s): 14.65.Ha, 12.38.Bx, 13.30.Ce, 13.88.+e

I. INTRODUCTION

In the decay of an unpolarized or polarized top quark to the W-gauge boson and a bottom quark the W^+ is strongly polarized, or, phrased in a different language, the W^+ has a nontrivial spin density matrix. Furthermore, the spin density matrix of the W can be tuned by changing the polarization of the top quark. The polarization of the W^+ will reveal itself in the angular decay distribution of its subsequent decays $W^+ \to l^+ + \nu_l$ (or $W^+ \to \bar{q} + q$).[1]

In the first stage one will aim to analyze the decay of unpolarized top quarks (or the average over its polarization). The decay distribution of unpolarized top-quark decay is governed by three structure functions, which we shall refer to as H_U (unpolarized transverse), H_L (longitudinal), and H_F (forward-backward asymmetric). In fact, the Collider Detector at Fermilab (CDF) Collaboration has already presented some results on the measurement of the longitudinal component of the W based on the limited run I data [1]. The measurement has confirmed the expected dominance of the longitudinal mode. The error on this measurement is quite large ($\approx 45\%$) but is expected to be reduced significantly during run II at the Fermilab Tevatron to start in the spring of 2001. In run II $(5-6)\times 10^3$ top quark pairs will be produced per year and detector. This number will be boosted to $10^7 - 10^8$ top quark pairs per year and detector at the CERN Large Hadron Collider (LHC) starting in 2006 or 2007. It is conceivable that the errors on the structure function measurements can be reduced to the 1–2% level in the next few years [2]. If such an accuracy can, in fact, be achieved, and having in mind that the $O(\alpha_s)$ corrections to the top-quark decay rate amount to 8.5% [3–8], it is quite evident that one needs to improve on the known theoretical Born level predictions for the above three structure functions by calculating their next-to-leading order radiative corrections.

At a later stage, when the data sample of polarized top quarks has become sufficiently large, one will also be able to analyze the decays of polarized top quarks. The top quark is very short lived and therefore retains its full polarization content when it decays. Polarized top quark decay brings in five additional polarized structure functions which can be measured through an analysis of spin-momentum correlations between the polarization vector of the top quark and the momenta of its decay products.

Polarized top quarks will become available at hadron colliders through single top-quark production, which occurs at the 33% level of the top-quark pair production rate [9]. Future e^+e^- colliders will also be copious sources of polarized top-quark pairs [10–15]. For example, at the proposed DESY TeV Energy Superconducting Linear Accelerator (TESLA) one expects rates of $(1-4)\times 10^5$ top-quark pairs per year. The polarization of these can easily be tuned through the availability of polarized beams (see, e.g., [16]). Further, there is a high degree of correlation between the polarization of top and quarks and antiquarks produced in pairs either at e^+e^- colliders [17–20] or at hadron colliders [21], which can be probed through the joint decay distributions of the top quark and antiquark.

In this paper we study momentum-momentum and spin-momentum correlations in the cascade decay process $t \to W^+ + b$ followed by $W^+ \to l^+ + \nu_l$. The step-1 decay $t \to W^+ + b$ is analyzed in the t rest frame where we study the spin-momentum correlation between the spin of the top quark and the momentum of the W. In step 2 we go to the rest frame of the W and analyze the correlation between the momentum of the lepton (or antiquark) and the initial momentum direction of the W. In technical terms this means we analyze the double density matrix of the decaying top quark

[1]From this point on we shall drop explicit reference to the $W^+ \to \bar{q} + q$ decay channel since it has the same angular decay distribution as $W^+ \to l^+ + \nu_l$. In fact the branching fraction into the two hadronic channels $(\bar{d} + u)$ and $(\bar{s} + c)$ exceeds that of the sum of the three leptonic channels by a factor of approximately 2 because of the color enhancement factor. Although not explicitly mentioned further on, the existence of the hadronic decay mode of the W^+ is always implicitly assumed in the following.

and the *W*-gauge boson produced. This must be contrasted with the *center of mass* analysis of polarized top-quark decay where the spin-momentum correlations are all analyzed in the rest system of the top quark [for an $O(\alpha_s)$ analysis of this kind, see [22]]. Experimentally such a correlation measurement is easier, but from a theoretical point of view the cascade type of analysis is advantageous because one can then better isolate the contribution of the longitudinal mode of the *W*-gauge boson, which is of relevance for understanding the electroweak symmetry breaking sector in the standard model. The results of the two analyses are of course related through a Lorentz boost along the *W* direction. However, the azimuthal correlations to be discussed later are not affected by such a Lorentz boost and are thus identical in both types of analysis.

The complete angular decay distribution is governed by altogether eight structure functions which we calculate analytically, including their full $O(\alpha_s)$ radiative corrections. One of the motivations for calculating the $O(\alpha_s)$ radiative corrections is the fact that the radiative QCD corrections populate helicity configurations that are not accessible at the Born level. Take, for example, unpolarized top-quark decay where, at the Born level, the W^+ cannot be right handed, i.e., it cannot have positive helicity, due to angular momentum conservation when $m_b=0$. This implies that strictly forward l^+ production does not occur at the Born level. However, when radiative corrections are taken into account, right-handed *W*'s do occur and strictly forward l^+ production is allowed. As we shall see in Sec. IV, technically this means that the structure function combination $(H_U+H_F)/2$ vanishes at the Born term level but becomes nonzero at $O(\alpha_s)$ [23]. We shall, however, see that the $O(\alpha_s)$ population of the right-handed *W* is rather small [23]. The same statement holds true for the other structure function combinations that vanish at the Born term level.

In order to retain full control over the *b*-mass dependence, and having also other applications in mind, we have kept a finite mass value for the *b* quark in our calculation. This improves on our earlier calculation of polarized top-quark decay where the *b*-quark mass was neglected and where we limited our attention to the six (diagonal) structure functions that govern the polar angle distribution in cascade decay [16]. The additional two (nondiagonal) structure functions calculated in this paper describe the azimuthal correlation of the plane of the top quark's polarization and the plane defined by the final leptons. In addition, we determine the unpolarized and polarized scalar structure functions, which are of relevance in the analysis of top-quark decay into a bottom quark and a charged Higgs boson [24]. We mention that our calculations have been done in the zero width approximation of the *W* boson. Finite width effects will be addressed in a forthcoming paper [25] (see also [26]).

Most of the results in this paper are new. They have been checked against limiting cases and partial results obtained in other papers. We have checked our analytical $O(\alpha_s)$ result for the total rate against the corresponding analytical rate result of Denner and Sack, who also kept the *b*-quark mass finite [3]. We find agreement. We took the zero *b*-quark mass limit of the six diagonal structure functions and obtained agreement with our previous results in [16]. These had already been checked against the analytical results for the total rate obtained in [4–7] and for the longitudinal/transverse composition obtained in [27]. All six (mass zero) diagonal structure functions had also been checked against the corresponding numerical results given in [27–29]. The unpolarized scalar structure function has been checked against the results of [24].

The central topic of this paper is the analysis of polarized top-quark decay. We therefore mostly limit our attention to results valid in the limit $m_b \to 0$ in the main part of our paper. This leads to enormous simplifications in the analytical rate formulas. The quality of the $m_b=0$ approximation may be judged from the Born term rate which increases by 0.27% on going from $m_b=4.8$ GeV to $m_b=0$. The full $m_b \neq 0$ structure is given in Sec. VIII and the Appendixes. Apart from retaining full control over $m_b \neq 0$ effects the finite mass results are needed, e.g., in the theoretical analysis of semileptonic $b \to c$ decays, where the *c*-quark mass can certainly not be neglected.

Our paper is structured as follows. In Sec. II we define a set of three spin independent and five spin dependent structure functions through the covariant expansion of the decay tensor resulting from the product of the two relevant current matrix elements. The eight invariant structure functions are related to eight helicity structure functions which form the angular coefficients of the angular decay distribution. In order to facilitate the calculation of the tree graph contributions we define a set of five covariant projection operators and a covariant representation of the spin vector of the top quark. These projectors can be used to covariantly project the requisite helicity structure functions from the hadron tensor. The advantage is that one thereby obtains the appropriate helicity structure functions and scalarizes the tensor integrands needed for the tree graph integration in one step. In Sec. III we derive the explicit form of the angular decay distribution in terms of the eight helicity structure functions for top quark decay. We also specify the changes in the angular decay distribution needed for top antiquark decay. Section IV contains our Born term results. In Sec. V we list our results for the $m_b=0$ one-loop contributions. In Sec. VI we provide expressions for the $O(\alpha_s)$ tree graph contributions and discuss technical details of how we have handled the necessary tree graph integrations. We mention that the infrared divergencies are regularized by a finite small gluon mass. In Sec. VII we take the $m_b \to 0$ limit of the $m_b \neq 0$ results in Sec. VIII and present rather compact analytical $O(\alpha_s)$ formulas for the various structure functions. Section VII also contains our numerical results in the $m_b=0$ approximation. Section VIII gives our analytical results on the tree graph integrations plus the one-loop contributions for $m_b \neq 0$. Section IX provides a summary and our conclusions. In particular, we emphasize that angular measurements as advocated in this paper can be utilized to measure the mass of the top quark. In Appendix A, we provide a complete list of $m_b \neq 0$ basis integrals that appear in the calculation of the tree graph contributions. This set of basis integrals should also be useful for other $O(\alpha_s)$ or $O(\alpha)$ radiative correction calculations. The requisite coefficient functions that multiply the basic integrals in the struc-

ture function expressions are listed in Appendix B. Appendix C, finally, contains the one-loop contribution in the $m_b \neq 0$ case.

II. INVARIANT AND HELICITY STRUCTURE FUNCTIONS

The dynamics of the current-induced $t \to b$ transition is embodied in the hadron tensor $H^{\mu\nu}$ which is defined by

$$H^{\mu\nu}(q_0, q^2 = m_W^2, s_t) = (2\pi)^3 \sum_{X_b} \int d\Pi_f \delta^4(p_t - q - p_{X_b}) \times \frac{1}{2m_t} \langle t(p_t, s_t)|J^{\nu +}|X_b\rangle \times \langle X_b|J^{\mu}|t(p_t, s_t)\rangle, \tag{1}$$

where $d\Pi_f$ stands for the Lorentz-invariant phase space factor. In the standard model the weak current is given by $J^{\mu} = \overline{q_b}\gamma^{\mu} P_L \overline{q_t}$ with $P_L = \frac{1}{2}(1 - \gamma_5)$.

We are working in the narrow resonance approximation of the W boson and set $q^2 = m_W^2$ as indicated in the argument of the hadron tensor. Thus the hadron tensor is a function of the energy q_0 of the W alone. Since we are not summing over the top-quark spin the hadron tensor also depends on the top-quark spin s_t as indicated in Eq. (1). The structure of the hadron tensor can be represented by a standard set of invariant structure functions defined by the expansion

$$\begin{aligned} H^{\mu\nu} = & (-g^{\mu\nu} H_1 + p_t^{\mu} p_t^{\nu} H_2 - i\epsilon^{\mu\nu\rho\sigma} p_{t,\rho} q_{\sigma} H_3) \\ & - (q \cdot s_t)(-g^{\mu\nu} G_1 + p_t^{\mu} p_t^{\nu} G_2 - i\epsilon^{\mu\nu\rho\sigma} p_{t,\rho} q_{\sigma} G_3) \\ & + (s_t^{\mu} p_t^{\nu} + s_t^{\nu} p_t^{\mu}) G_6 + i\epsilon^{\mu\nu\rho\sigma} p_{t\rho} s_{t\sigma} G_8 \\ & + i\epsilon^{\mu\nu\rho\sigma} q_{\rho} s_{t\sigma} G_9, \end{aligned} \tag{2}$$

where H_i $(i = 1,2,3)$ and G_i $(i = 1,2,3,6,8,9)$ denote unpolarized and polarized structure functions, respectively.

In the expansion (2) we have kept only those structure functions that contribute in the zero lepton mass case. We have thus omitted covariants built from q^{μ} and/or q^{ν}. We have also dropped contributions from invariants that are fed by T-odd or imaginary contributions, which are both absent in the present case.

In the expansion (2) one has still overcounted by one term since there is a relationship between the three parity-conserving (pc) spin dependent covariants appearing in Eq. (2) because of the identity of Schouten. The identity between the three covariants reads

$$q \cdot s_t \epsilon^{\mu\nu\rho\sigma} p_{t,\rho} q_{\sigma} - q^2 \epsilon^{\mu\nu\rho\sigma} p_{t,\rho} s_{t\sigma} + q \cdot p_t \epsilon^{\mu\nu\rho\sigma} q_{\rho} s_{t,\sigma} = 0. \tag{3}$$

We shall, however, keep the overcounted set of nine invariant structure functions in Eq. (2) for reasons of computational convenience.

In this paper we shall be concerned with only two types of intermediate state in Eq. (1), namely, $|X_b\rangle = |b\rangle$ [Born term and $O(\alpha_s)$ one-loop contributions] and $|X_b\rangle = |b + g\rangle$ $[O(\alpha_s)$ tree graph contribution]. The Feynman diagrams contributing to the respective processes are drawn in Fig. 1.

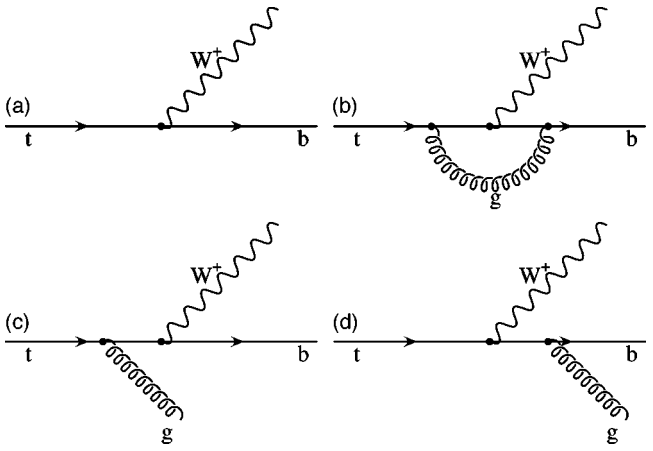

FIG. 1. Leading order Born term contribution (a) and $O(\alpha_s)$ contributions (b)–(d) to $t \to b + W^+$.

The angular decay distribution that we are aiming for is given in terms of a set of angular decay coefficients which are linearly related to the set of unpolarized structure functions H_i and polarized structure functions G_i defined in Eq. (2). The relevant linear combinations are given by

$$H_U = H_{++} + H_{--} = H_{11} + H_{22}, \tag{4a}$$

$$H_L = H_{00} = H_{33}, \tag{4b}$$

$$H_F = H_{++} - H_{--} = i(H_{12} - H_{21}), \tag{4c}$$

$$H_{U^P} = H_{++}(s_t^l) + H_{--}(s_t^l) = H_{11}(s_t^l) + H_{22}(s_t^l), \tag{4d}$$

$$H_{L^P} = H_{00}(s_t^l) = H_{33}(s_t^l), \tag{4e}$$

$$H_{F^P} = H_{++}(s_t^l) - H_{--}(s_t^l) = i[H_{12}(s_t^l) - H_{21}(s_t^l)], \tag{4f}$$

$$H_{I^P} = \tfrac{1}{4}[H_{+0}(s_t^{\rm tr}) + H_{0+}(s_t^{\rm tr}) - H_{-0}(s_t^{\rm tr}) - H_{0-}(s_t^{\rm tr})] \tag{4g}$$

$$= -\frac{1}{2\sqrt{2}}[H_{13}(s_t^{\rm tr}) + H_{31}(s_t^{\rm tr})], \tag{4h}$$

$$H_{A^P} = \tfrac{1}{4}[H_{+0}(s_t^{\rm tr}) + H_{0+}(s_t^{\rm tr}) + H_{-0}(s_t^{\rm tr}) + H_{0-}(s_t^{\rm tr})] \tag{4i}$$

$$= \frac{i}{2\sqrt{2}}[H_{23}(s_t^{\rm tr}) - H_{32}(s_t^{\rm tr})], \tag{4j}$$

where $H_{\lambda_W;\lambda'_W} = H_{\mu\nu}\epsilon^{*\mu}(\lambda_W)\epsilon^{\nu}(\lambda'_W)$ are the helicity projections of the polarized and unpolarized pieces of the structure functions $H^{\mu\nu}$. The $\epsilon^{*\mu}(\lambda_W)$ and $\epsilon^{\nu}(\lambda_W)$ are the usual spherical components of the polarization vector of the W-gauge boson. In the top-quark rest system with $q^{\mu} = (q_0; 0, 0, |\vec{q}|)$ and $|\vec{q}| = (q_0^2 - m_W^2)^{1/2}$ they read

$$\epsilon^{\mu}(0)=\frac{1}{m_W}(|\vec{q}|;0,0,q_0), \tag{5}$$

$$\epsilon^{\mu}(\pm)=\frac{1}{\sqrt{2}}(0;\mp 1,-i,0). \tag{6}$$

In Eqs. (4a)–(4j) we have also included the Cartesian components of the helicity structure functions in the *W*-boson rest frame, which are useful for some applications. For notational convenience we shall often refer to the set of helicity structure functions by their generic names. Thus we shall frequently use U for H_U and U^P for H_{U^P}, etc.

The rest frame components of the longitudinal ("*l*") and transverse ("tr") polarization vector of the top quark are simply given by $s_t^l=(0;0,0,1)$ and $s_t^{\rm tr}=(0;1,0,0)$. For the unpolarized helicity structure functions one sums over the two diagonal spin configurations of the top quark while one takes the differences of these for the polarized helicity structure functions (in the *z* basis for s_t^l and in the *x* basis for $s_t^{\rm tr}$). When computing the polarized structure functions from the relevant Dirac trace expressions one thus has to replace $(\not{p}_t+m_t)$ in the unpolarized Dirac string by $(\not{p}_t+m_t)(1+\gamma_5\not{s}_t)$. Note that the longitudinal component contributes only to the diagonal helicity structure functions U, L, and F while the transverse component contributes only to the nondiagonal structure functions I and A. The physics behind this will become clear when we write down the angular decay distribution in Sec. III.

It turns out that it is rather convenient from the computational point of view to represent the helicity projections in Eqs. (4a)–(4j) (defined by the gauge-boson polarization vectors and the top-quark polarization vector) in covariant form. One has

$$H_i=H_{\mu\nu}\mathbb{P}_i^{\mu\nu}, \quad i=U,L,F, \tag{7a}$$

$$H_{i^P}=H_{\mu\nu}(s_t^l)\mathbb{P}_i^{\mu\nu}, \quad i=U,L,F, \tag{7b}$$

$$H_{i^P}=H_{\mu\nu}(s_t^{\rm tr})\mathbb{P}_i^{\mu\nu}, \quad i=I,A. \tag{7c}$$

The covariant projectors onto the diagonal density matrix elements are given by

$$\mathbb{P}_L^{\mu\nu}=\frac{m_W^2}{m_t^2}\frac{1}{|\vec{q}|^2}\left(p_t^u-\frac{p_t\cdot q}{m_W^2}q^{\mu}\right)\left(p_t^{\nu}-\frac{p_t\cdot q}{m_W^2}q^{\nu}\right), \tag{8a}$$

$$\mathbb{P}_{U+L}^{\mu\nu}=-g^{\mu\nu}+\frac{q^{\mu}q^{\nu}}{M_W^2}, \tag{8b}$$

$$\mathbb{P}_F^{\mu\nu}=\frac{1}{m_t}\frac{1}{|\vec{q}|}i\epsilon^{\mu\nu\alpha\beta}p_{t,\alpha}q_{\beta}, \tag{8c}$$

where $\epsilon^{0123}=-1$. We do not write out the projector for the unpolarized transverse component U but note that it can be obtained from the combination $\mathbb{P}_{U+L}^{\mu\nu}-\mathbb{P}_L^{\mu\nu}$.

The projectors onto the transverse-longitudinal nondiagonal density matrix elements are given by

$$\mathbb{P}_I^{\mu\nu}=+\frac{1}{2\sqrt{2}}\frac{m_W}{m_t}\frac{1}{|\vec{q}|}\left\{\epsilon^{\mu}(x)\left(p_t^{\nu}-\frac{p_t\cdot q}{m_W^2}q^{\nu}\right)+\mu\leftrightarrow\nu\right\}, \tag{8d}$$

$$\mathbb{P}_A^{\mu\nu}=-\frac{1}{2\sqrt{2}}\frac{m_W}{m_t^2}\frac{1}{|\vec{q}|^2}\left\{i\epsilon^{\nu m\alpha\beta\gamma}\epsilon_{\alpha}(x)p_{t,\beta}q_{\gamma}\times\left(p_t^{\nu}-\frac{p_t\cdot q}{m_W^2}q^{\nu}\right)-\mu\leftrightarrow\nu\right\}. \tag{8e}$$

They involve the the transverse polarization vector of the *W*-gauge boson $\epsilon_{\alpha}(x)=(0;1,0,0)$ pointing in the *x* direction.

The covariant representation of the longitudinal component of the polarization vector of the top-quark spin vector s_t^l is given by

$$s_t^{l,\mu}=\frac{1}{|\vec{q}|}\left(q^{\mu}-\frac{p_t\cdot q}{m_t^2}p_t^{\mu}\right), \tag{9}$$

whereas its transverse component $s_t^{\rm tr}$ reads

$$s_t^{{\rm tr},\mu}=(0;1,0,0). \tag{10}$$

Note the inverse powers of $|\vec{q}|=\sqrt{q_0^2-m_W^2}$ that enter the L, T, F, I, and A projectors and the longitudinal polarization vector. They come in for normalization reasons. These inverse powers of $|\vec{q}|$ will make the necessary tree graph integrations to be dealt with in Sec. VI and in the Appendixes A and B somewhat more complicated than the total $(U+L)$ rate integration, which has a rather simple projector as Eq. (8b) shows.

As mentioned in the Introduction, the covariant forms of the projection operators (8a)–(8e) and the polarization vectors (9) and (10) are quite convenient for the calculation of the $O(\alpha_s)$ tree graph contributions to be dealt with in Sec. VI. The covariant projectors allow one to scalarize the tree graph tensor integrands and to project onto the requisite helicity structure functions in one step.

Although we shall mostly work in the helicity representation of the structure functions, it is sometimes convenient to have available the set of linear relations between the helicity and invariant structure functions. These can easily be worked out from the expansion (2), the projectors (8a)–(8e), and the polarization vectors (10). One has

$$H_U=2H_1, \tag{11a}$$

$$m_W^2H_L=m_W^2H_1+|\vec{q}|^2m_t^2H_2, \tag{11b}$$

$$H_F=2|\vec{q}|m_tH_3, \tag{11c}$$

$$H_{U^P}=2|\vec{q}|G_1, \tag{11d}$$

$$m_W^2H_{L^P}=|\vec{q}|(m_W^2G_1+|\vec{q}|^2m_t^2G_2-2q_0m_tG_6), \tag{11e}$$

$$H_{F^P}=2|\vec{q}|^2m_tG_3-2m_tG_8-2q_0G_9, \tag{11f}$$

$$H_{I^P}=\frac{1}{\sqrt{2}}\frac{m_t}{m_W}|\vec{q}|G_6, \tag{11g}$$

$$H_{A^P}=-\frac{1}{\sqrt{2}}\frac{m_t q_0}{m_W}G_8-\frac{1}{\sqrt{2}}m_W G_9. \tag{11h}$$

Note that the three structure functions G_3, G_8, and G_9 always contribute in the two combinations $(m_W^2 G_3+G_8)$ and $(q_0 m_1 G_3-G_9)$, proving again that there are only eight independent combinations of structure functions. If desired, Eqs. (11a)–(11h) can be inverted such that the invariant structure functions can be expressed in terms of the helicity structure functions. The inversion has to be done in terms of the two above linear combinations of G_3, G_8, and G_9. Since our later results will always be presented in terms of the helicity structure functions, we shall not write down the inverse relations here.

III. ANGULAR DECAY DISTRIBUTION

We are now in the position to write down the full angular decay distribution of polarized top-quark decay into W^+ and b followed by the decay of the W^+ into $(l^+ + \nu_l)$. As noted before, the full angular decay distribution of the decay $t(\uparrow) \to W^+(\to l^+ + \nu_l)+X_b$, including polarization effects of the top quark, is completely determined by the three unpolarized and five polarized helicity structure functions. Although the necessary manipulations to obtain the angular decay distribution involving Wigner's $D^J_{mm'}(\theta,\phi)$ functions are standard (see, e.g., [30]), it is quite instructive to reproduce the results here. To this end, it is useful to define helicity structure functions $H^{\lambda_t\lambda_t'}_{\lambda_W\lambda_W'}$ where the helicity label of the top quark is made explicit. Put in a different language, the four-index object $H^{\lambda_t\lambda_t'}_{\lambda_W\lambda_W'}$ is the unnormalized double density matrix of the top quark and the W. The double density matrix is Hermitian; i.e., it satisfies

$$\left(H^{\lambda_t\lambda_t'}_{\lambda_W\lambda_W'}\right)^*=\left(H^{\lambda_t'\lambda_t}_{\lambda_W'\lambda_W}\right). \tag{12}$$

As has been remarked on before, the elements of the double density matrix are real in the present application. The double density matrix is therefore symmetric. The relation of the components of the double density matrix to the previously defined unpolarized and polarized helicity structure functions is given by

$$H_U=H^{++}_{++}+H^{--}_{++}+H^{++}_{--}+H^{--}_{--}, \tag{13a}$$

$$H_L=H^{++}_{00}+H^{--}_{00}, \tag{13b}$$

$$H_F=H^{++}_{++}+H^{--}_{++}-H^{++}_{--}-H^{--}_{--}, \tag{13c}$$

$$H_{U^P}=H^{++}_{++}-H^{--}_{++}+H^{++}_{--}-H^{--}_{--}, \tag{13d}$$

$$H_{L^P}=H^{++}_{00}-H^{--}_{00}, \tag{13e}$$

$$H_{F^P}=H^{++}_{++}-H^{--}_{++}-H^{++}_{--}+H^{--}_{--}, \tag{13f}$$

$$H_{I^P}=\tfrac{1}{4}(H^{+-}_{+0}+H^{-+}_{0+}-H^{-+}_{-0}-H^{+-}_{0-})$$
$$=\tfrac{1}{2}(H^{+-}_{+0}-H^{-+}_{-0}), \tag{13g}$$

$$H_{A^P}=\tfrac{1}{4}(H^{+-}_{+0}+H^{-+}_{0+}+H^{-+}_{-0}+H^{+-}_{0-})$$
$$=\tfrac{1}{2}(H^{+-}_{+0}+H^{-+}_{-0}). \tag{13h}$$

For ease of notation we have used $(\pm)$ labels for both the helicities of the top quark $(\lambda_t=\pm 1/2)$ and the transverse helicities of the W-gauge boson $(\lambda_W=\pm 1)$. In the case of the nondiagonal structure functions H_{I^P} and H_{A^P} one can make use of the fact that the double density matrix is symmetric (for real coefficients) to simplify the structure functions as indicated in the last two lines of Eqs. (13g)–(13h). From the fact that we are not observing the spin of the X_b system in our semi-inclusive measurement one has $\lambda_{X_b}=\lambda'_{X_b}$, leading to the constraint $\lambda_W-\lambda'_W=\lambda_t-\lambda'_t$. From this constraint it is immediately clear that the polarized structure functions U, L, and F are associated with the longitudinal spin of the top quark and the structure functions I and A are associated with the transverse spin of the top quark.

The angular decay distribution can be obtained from the master formula

$$W(\theta_P,\theta,\phi)\propto \sum_{\lambda_W-\lambda'_W=\lambda_t-\lambda'_t} e^{i(\lambda_W-\lambda'_W)\phi} d^1_{\lambda_W 1}(\theta)$$
$$\times d^1_{\lambda'_W 1}(\theta) H^{\lambda_t\lambda'_t}_{\lambda_W\lambda'_W}\rho_{\lambda_t\lambda'_t}(\theta_P), \tag{14}$$

where $\rho_{\lambda_t\lambda'_t}(\theta_P)$ is the density matrix of the top quark which reads

$$\rho_{\lambda_t\lambda'_t}(\theta_P)=\frac{1}{2}\begin{pmatrix} 1+P\cos\theta_P & P\sin\theta_P \\ P\sin\theta_P & 1-P\cos\theta_P \end{pmatrix}. \tag{15}$$

P is the magnitude of the polarization of the top quark. The sum in Eq. (14) extends over all values of λ_W, λ'_W, λ_t, and λ'_t compatible with the constraint $\lambda_W-\lambda'_W=\lambda_t-\lambda'_t$. The second lower index in the small Wigner $d(\theta)$ function $d^1_{\lambda_W 1}$ is fixed at $m=1$ for zero mass leptons because the total m quantum number of the lepton pair along the l^+ direction is $m=1$. Because there exist different conventions for Wigner's d functions we explicate the requisite components that enter Eq. (14): $d^1_{11}=(1+\cos\theta)/2$, $d^1_{01}=\sin\theta/\sqrt{2}$, and $d^1_{-11}=(1-\cos\theta)/2$.

Including the appropriate normalization factor the four-fold decay distribution is given by

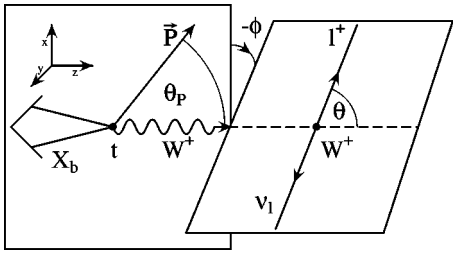

FIG. 2. Definition of the polar angles θ and θ_P and the azimuthal angle ϕ. $\vec{P}$ is the polarization vector of the top quark.

$$\frac{d\Gamma}{dq_0 d\cos\theta_P d\cos\theta\, d\phi} = \frac{1}{4\pi}\frac{G_F|V_{tb}|^2 m_W^2}{\sqrt{2}\pi}|\vec{q}|\Big\{\frac{3}{8}(H_U + P\cos\theta_P H_{U^P})\times(1+\cos^2\theta) + \frac{3}{4}(H_L + P\cos\theta_P H_{L^P})\sin^2\theta + \frac{3}{4}(H_F + P\cos\theta_P H_{L^P})\cos\theta + \frac{3}{2\sqrt{2}}P\sin\theta_P H_{I^P}\sin 2\theta\cos\phi + \frac{3}{\sqrt{2}}P\sin\theta_P H_{A^P}\sin\theta\cos\phi\Big\}. \quad (16)$$

We take the freedom to normalize the differential rate such that one obtains the total $t\to b+W^+$ rate upon integration and not the total rate multiplied by the branching ratio of the corresponding W^+ decay channel.

The polar angles θ_P and θ and the azimuthal angle ϕ that arise in the full cascade-type description of the two-stage decay process $t(\uparrow)\to W^+(\to l^+ + \nu_l) + X_b$ are defined in Fig. 2. For better visibility we have oriented the lepton plane with a negative azimuthal angle relative to the hadron plane. For the hadronic decays of the W into a pair of light quarks one has to replace (l^+,ν_l) by $(\bar{q},q)$ in Fig. 2. We mention that we have checked the signs of the angular decay distribution Eq. (16) using covariant techniques.

As Eq. (16) shows, the nondiagonal structure functions H_{I^P} and H_{A^P} are associated with azimuthal measurements. This necessitates the definition of a hadron plane, which is only possible through the availability of the x component of the polarization vector of the top (see Fig. 2). This is the physical explanation of why the two structure functions H_{I^P} and H_{A^P} are functions of only the transverse component of the polarization vector of the top quark. For similar reasons the polarization dependent structure functions H_{U^P}, H_{L^P}, and H_{F^P} depend only on the longitudinal component of the polarization vector.

Setting $P=0$ in Eq. (16) one obtains the decay distribution for unpolarized top-quark decay. If desired, the transverse part of the unpolarized angular decay distribution can also be sorted in terms of decays into transverse-plus and transverse-minus W bosons given by the structure function combinations $(U+F)/2$ and $(U-F)/2$, which multiply the angular factors $(1+\cos\theta)^2$ and $(1-\cos\theta)^2$, respectively, as was done, e.g., in [23].

If there were an imaginary part in the one-loop contribution one would have two additional contributions to the angular decay distribution proportional to $\sin\phi$. This can be easily seen with the help of Eq. (14). We concentrate on those terms in the angular decay distribution that are proportional to the off-diagonal terms ρ_{+-} in the density matrix of the top quark. The relevant terms read

$$H_{+0}^{+-}e^{+i\phi} + H_{0+}^{-+}e^{-i\phi} = 2[\mathrm{Re}(H_{+0}^{+-})\cos\phi - \mathrm{Im}(H_{+0}^{+-})\sin\phi], \quad (17a)$$

$$H_{0-}^{+-}e^{+i\phi} + H_{-0}^{-+}e^{-i\phi} = 2[\mathrm{Re}(H_{0-}^{+-})\cos\phi - \mathrm{Im}(H_{0-}^{+-})\sin\phi]. \quad (17b)$$

The real contributions multiplying the angular factor $\cos\phi$ have been included in the angular decay distribution (16) while the imaginary contributions $\mathrm{Im}(H_{+0}^{+-})$ and $\mathrm{Im}(H_{0-}^{+-})$ multiplying $\sin\phi$ do not appear in Eq. (16) since the $O(\alpha_s)$ contributions calculated in this paper are purely real. The helicity structure functions $\mathrm{Im}(H_{+0}^{+-})$ and $\mathrm{Im}(H_{0-}^{+-})$ are conventionally called T-odd structure functions and are contributed to by the imaginary parts of loop contributions and/or by CP-violating contributions which, as has been emphasized before, are not present in this calculation.

Of interest is also the corresponding angular decay distribution for polarized top-antiquark decay $\bar{t}(\uparrow)\to W^-(\to l^- + \bar{\nu}_l) + X_b^-$. The angular decay distribution is changed due to the fact that the total m quantum number of the lepton pair in the l^- direction is now $m=-1$. The relevant components of the small Wigner d function are now $d^1_{1-1}=(1-\cos\theta)/2$, $d^1_{0-1}=-\sin\theta/\sqrt{2}$ and $d^1_{-1-1}=(1+\cos\theta)/2$. This can be seen to result in a sign change for the angular factors multiplying the F, F^P, and A^P terms (and no sign change for the other terms). The structure functions of top-antiquark decay are related to those of top decay by CP invariance. The parity-violating (PV) structure functions F, U^P, L^P, and I^P will undergo a sign change whereas parity-conserving (PC) structure functions U, L, F^P, and A^P keep their signs. Overall this means that the unpolarized terms in Eq. (16) will not change their signs while the polarized terms will change signs when going from top-quark decay to top-antiquark decay. To be quite explicit, if one wants to use the results of this paper to describe top-antiquark decay, the only required effective change is to change the signs of the terms multiplying the U^P, L^P, F^P, I^P, and A^P structure functions in the angular decay distribution Eq. (16), using, however, the same structure functions as written down in this paper.

IV. BORN TERM RESULTS

The Born term tensor is calculated from the square of the Born term amplitude [see Fig. 1(a)] given by

$$M^{\mu}=V_{tb}=\frac{g}{\sqrt{2}}\overline{u}_b\gamma^{\mu}\frac{1}{2}(1-\gamma_5)u_t. \tag{18}$$

We omit the coupling factor $V_{tb}g/\sqrt{2}=2m_W V_{tb}(G_F/\sqrt{2})^{1/2}$ and write for the Born term tensor (the spin of the b quark is summed)

$$B^{\mu\nu}=\tfrac{1}{4}\mathrm{Tr}(\not{p}_b+m_b)\gamma^{\mu}(1-\gamma_5)(\not{p}_t+m_t)\times(1+\gamma_5\not{s}_t)\gamma^{\nu}(1-\gamma_5). \tag{19}$$

Since only even-numbered γ-matrix strings survive between the two $(1-\gamma_5)$ factors in Eq. (19) one can compactly write

$$B^{\mu\nu}=2(\overline{p}_t^{\nu}p_b^{\mu}+\overline{p}_t^{\mu}p_b^{\nu}-g^{\mu\nu}\overline{p}_t\cdot p_b+i\epsilon^{\mu\nu\alpha\beta}p_{b,\alpha}\overline{p}_{t,\beta}), \tag{20}$$

where

$$\overline{p}_t^{\mu}=p_t^{\mu}-m_t s_t^{\mu}. \tag{21}$$

It is not difficult to obtain the Born term helicity structure functions from Eq. (20). This can be done in two ways. One can read off the invariant structure functions according to the covariant expansion Eq. (2). The nonvanishing elements are given by $B_{H_1}=m_t^2(1-x^2+y^2)$, $B_{H_2}=-2B_{H_3}=4$ for the unpolarized invariants and by $B_{G_1}=B_{G_6}=B_{G_8}=-B_{G_9}=-2m_t$ for the polarized invariants (the notation is self-explanatory). These can then be converted to the helicity structure functions using the linear relations (11a)–(11h). Alternatively one can directly compute the helicity structure functions from Eq. (20) by using the covariant projectors defined in Sec. II [cf. Eqs. (8a)–(8e)].

In order to find the relation of the Born term tensor $B^{\mu\nu}$ to the hadron tensor $H^{\mu\nu}$ defined in Sec. II one has to insert the appropriate one-particle b-quark state into Eq. (1) and then one has to do the requisite one-particle phase space integration. Technically this is done by rewriting the one-particle phase space as

$$\int d\Pi_b=\int\frac{d^3\vec{p}_b}{2E_b}=\int d^4p_b\,\delta(p_b^2-m_b^2). \tag{22}$$

One can easily do the four-dimensional d^4p_b integration in Eq. (1) with the help of the four-dimensional δ function $\delta^4(p_t-q-p_b)$. This converts p_b^2 in the argument of the δ function in Eq. (22) into $(p_t-q)^2$. Rewriting the argument of the δ function in terms of q_0 one finally arrives at

$$H^{\mu\nu}(\mathrm{Born})=\frac{1}{4m_t^2}\,\delta\left(q_0-\frac{m_t^2+m_W^2-m_b^2}{2m_t}\right)B^{\mu\nu}. \tag{23}$$

We will present our results in table form where we use the scaled variables $x=m_W/m_t$ and $y=m_b/m_t$ as well as the abbreviation $|\vec{q}|=(m_t/2)\sqrt{\lambda}$ with $\lambda=\lambda(1,x^2,y^2)=1+x^4+y^4-2x^2y^2-2x^2-2y^2$. The first column in Table I contains the $m_b\neq 0$, or, equivalently, $y\neq 0$ results. In the second column we have set $m_b=0$ $(y=0)$. In order to assess the quality of the $m_b=0$ approximation for the various rate functions we have listed the percentage increments when going from the $m_b\neq 0$ case to the $m_b=0$ case *including* the phase space factor $|\vec{q}|$ that multiplies the helicity structure functions in the rate formula Eq. (16). In this comparison we have used $m_b=4.8$ GeV [31] together with $m_t=175$ GeV and $m_W=80.419$ GeV. The increment due to the phase space factor $|\vec{q}|$ alone amounts to 0.15%. Note that one may have overestimated the mass effect since a fixed pole mass, rather than a running mass which is smaller at the high scale of the top-quark mass, is used. For example, taking one-loop running and the same bottom pole mass as above one has $\overline{m}_b(m_t)=1.79$ GeV. The increment in the total rate on going from $\overline{m}_b(m_t)=1.79$ GeV to $m_b=0$ would then be only 0.04% as compared to the 0.26% given in Table I.

In the $m_b=0$ case listed in column 3 of Table I one observes the simple patterns $B_U=-B_{U^P}=-B_F=B_{F^P}$, $B_L=B_{L^P}$, and $B_{I^P}=-B_{A^P}$. This pattern results from the fact that a massless b quark emerging from a $(V-A)$ vertex is purely left handed. Since from angular momentum conservation one has $\lambda_t=\lambda_W-\lambda_b$ with $\lambda_b=-1/2$ one has the constraint $\lambda_t-\lambda_W=1/2$. This implies that only the helicity configurations $(\lambda_t=-1/2;\lambda_W=-1)$ and $(\lambda_t=+1/2;\lambda_W=0)$ are nonvanishing. A quick look at the relations (13a)–(13h) allows one to readily verify the $m_b=0$ pattern in Table I. For $m_b\neq 0$ there is a leakage into right-handed bottom mesons resulting in a breaking of the above pattern as can be observed in the $m_b\neq 0$ column of Table I. As noted in the Introduction these simple patterns are also not valid at $O(\alpha_s)$ even for massless bottom mesons because of the additional gluon emission, including an anomalous spin-flip contribution [32]. When the relevant $m_b=0$ Born term helicity structure functions from Table I are substituted in Eq. (16) we reproduce the angular decay distribution as written down in [17].

For completeness we have also included the two Born term scalar helicity structure functions B_S and B_{S^P} in Table I. They are obtained by use of the scalar projector $\mathbb{P}_S=q^{\mu}q^{\nu}/m_W^2$. That they are identical to their longitudinal counterparts B_L and B_{L^P} even for $m_b\neq 0$ is a dynamical accident specific to the Born term level and does not hold true in general as, e.g., evidenced by the $O(\alpha_s)$ contributions to be discussed later on. These become equal to each other only in the limit $m_t\to\infty$ as will be discussed in Sec. VII. The $m_b\neq 0$ Born term equalities $B_F=B_{U^P}$ and $B_U=B_{F^P}$ can be seen to result from the fact that the double density matrix elements H_{++}^{--} and H_{--}^{++} vanish at the Born term level due to angular momentum conservation [see Eq. (13a)].

In Fig. 3 we present a Lego plot of the twofold $(m_b=0)$ Born term angular decay distribution in $\cos\theta$ and $\cos\theta_P$ which results after taking the azimuthal average of Eq. (16). We have divided out the total Born term rate from the differential rate, resulting in the careted differential rate distribution as defined in Eq. (35). We have set $P=1$ in Fig. 3. The Lego plot shows that the $\cos\theta$ and $\cos\theta_P$ variation of the twofold angular decay distribution around its average value of 0.25 is quite strong. This will facilitate the experimental measurement of the structure functions Γ_U, Γ_L, Γ_F, Γ_{U^P}, Γ_{L^P}, and Γ_{F^P}.

TABLE I. Born term helicity structure functions B_i $(i=U+L,U^P+L^P,U,U^P,L,L^P,F,F^P,S,S^P,I^P,A^P)$ for $m_b\neq 0$ and $m_b=0$. Fourth column gives the percentage increment when going from $m_b\neq 0$ to $m_b=0$ including the phase space factor $|\vec{q}|$.

Born term	$m_b\neq 0$	$m_b=0$	Increment
B_{U+L}	$m_t^2\frac{1}{x^2}[(1-y^2)^2+x^2(1-2x^2+y^2)]$	$m_t^2\frac{1}{x^2}(1-x^2)(1+2x^2)$	+0.27%
$B_{U^P+L^P}$	$m_t^2\sqrt{\lambda}\frac{1}{x^2}(1-2x^2-y^2)$	$m_t^2\frac{1}{x^2}(1-x^2)(1-2x^2)$	+0.42%
B_U	$2m_t^2(1-x^2+y^2)$	$2m_t^2(1-x^2)$	+0.05%
B_{U^P}	$-2m_t^2\sqrt{\lambda}$	$-2m_t^2(1-x^2)$	+0.29%
B_L	$m_t^2\frac{1}{x^2}[(1-y^2)^2-x^2(1+y^2)]$	$m_t^2\frac{1}{x^2}(1-x^2)$	+0.36%
B_{L^P}	$m_t^2\sqrt{\lambda}\frac{1}{x^2}(1-y^2)$	$m_t^2\frac{1}{x^2}(1-x^2)$	+0.37%
B_F	$-2m_t^2\sqrt{\lambda}$	$-2m_t^2(1-x^2)$	+0.29%
B_{F^P}	$2m_t^2(1-x^2+y^2)$	$2m_t^2(1-x^2)$	+0.05%
B_S	$m_t^2\frac{1}{x^2}[(1-y^2)^2-x^2(1+y^2)]$	$m_t^2\frac{1}{x^2}(1-x^2)$	+0.36%
B_{S^P}	$m_t^2\sqrt{\lambda}\frac{1}{x^2}(1-y^2)$	$m_t^2\frac{1}{x^2}(1-x^2)$	+0.37%
B_{I^P}	$-\frac{1}{1}\sqrt{2}m_t^2\sqrt{\lambda}\frac{1}{x}$	$-\frac{1}{2}\sqrt{2}m_t^2\frac{1}{x}(1-x^2)$	+0.29%
B_{A^P}	$\frac{1}{2}\sqrt{2}m_t^2\frac{1}{x}(1-x^2-y^2)$	$\frac{1}{2}\sqrt{2}m_t^2\frac{1}{x}(1-x^2)$	+0.24%

Finally, for the sake of definiteness we list the Born term rate in terms of the Born term function B_{U+L}. One has

$$\Gamma_0=\frac{G_F m_W^2|\vec{q}|}{4\sqrt{2}\pi m_t^2}|V_{tb}|^2 B_{U+L}. \tag{24}$$

V. ONE-LOOP CONTRIBUTION

The one-loop contributions to fermionic $(V-A)$ transitions have a long history. Since QED and QCD have the same structure at the one-loop level the history even dates back to QED times.

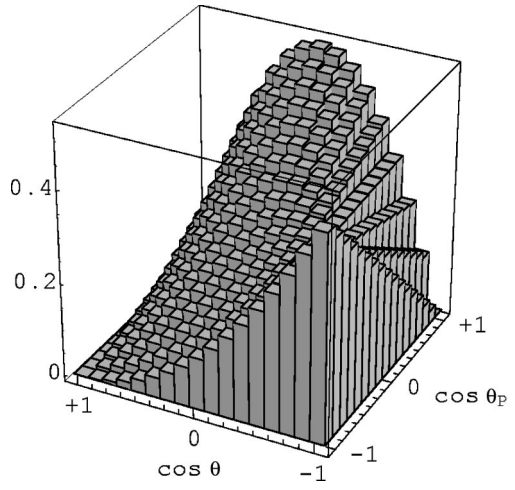

FIG. 3. Born term Lego plot of the twofold angular decay distribution $d\hat{\Gamma}/d\cos\theta\, d\cos\theta_P$ with $P=1$.

Our reference will be the work of Gounaris and Paschalis [34] (see also [33]) who used a gluon mass regulator to regularize the gluon IR singularity. The one-loop amplitudes are defined by the covariant expansion $(J_\mu^V=\overline{q}_b\gamma_\mu q_t, J_\mu^A=\overline{q}_b\gamma_\mu\gamma_5 q_t)$

$$\langle b(p_b)|J_\mu^V|t(p_t)\rangle=\overline{u}_b(p_b)\{\gamma_\mu F_1^V+p_{t,\mu}F_2^V+p_{b,\mu}F_3^V\}u_t(p_t), \tag{25a}$$

$$\langle b(p_b)|J_\mu^A|t(p_t)\rangle=\overline{u}_b(p_b)\{\gamma_\mu F_1^A+p_{t,\mu}F_2^A+p_{b,\mu}F_3^A\}\times\gamma_5 u_t(p_t). \tag{25b}$$

In the standard model the appropriate current combination is given by $J_\mu^V-J_\mu^A$.

We shall immediately take the limit $m_b\to 0$ of the one-loop expressions given in [34] (see also Appendix C).[2] Keeping only the finite terms and the relevant mass (M) $(\ln y$ and $\ln^2 y)$ and infrared $[\ln(\Lambda^2)]$ singular logarithmic terms one obtains the rather simple result

[2]We have recalculated the one-loop results of Ref. [34] and have found an acknowledged typo in the scalar form factors $F_3(Q^2)$ and $H_3(Q^2)$ of [34]. The typo is corrected by replacing the factor $(m_2-m_1)/Q^2$ in the last line of Eq. (A.8) of Ref. [34] by $(m_2-m_1)/(2Q^2)$.

$$F_1^V = F_1^A = 1 - \frac{\alpha_s(q^2)}{4\pi} C_F \Bigg[4 + \frac{1}{x^2}\ln(1-x^2) + \ln\left(\frac{y}{1-x^2}\frac{\Lambda^4}{(1-x^2)^2}\right) + 2\ln\left(\frac{\Lambda^2}{y}\frac{1}{1-x^2}\right) \times \ln\left(\frac{y}{1-x^2}\right) + 2\,\mathrm{Li}_2(x^2)\Bigg], \tag{26a}$$

$$F_2^V = -F_2^A = \frac{1}{m_t}\frac{\alpha_s(q^2)}{4\pi} C_F \frac{2}{x^2}\left(+1 + \frac{1-x^2}{x^2}\ln(1-x^2)\right), \tag{26b}$$

$$F_3^V = -F_3^A = \frac{1}{m_t}\frac{\alpha_s(q^2)}{4\pi} C_F \frac{2}{x^2}\left(-1 + \frac{2x^2-1}{x^2}\ln(1-x^2)\right), \tag{26c}$$

where we have denoted the scaled gluon mass by $\Lambda = m_g/m_t$. The dilogarithmic function $\mathrm{Li}_2(x)$ is defined by

$$\mathrm{Li}_2(x) := -\int_0^x \frac{\ln(1-z)}{z}\,dz. \tag{27}$$

Note that the one-loop contribution is purely real. This can be understood from an inspection of the one-loop Feynman diagram Fig. 1(b), which does not admit any nonvanishing physical two-particle cut. The fact that one has $F_1^V = F_1^A$ and $F_i^V = -F_i^A$ for $i=2,3$ results from setting the b-quark mass to zero. This can be seen by moving the chiral $(1-\gamma_5)$ factor in the one-loop integrand numerator to the left. Because m_b is set to zero the Dirac numerator string will thus begin with $\bar{u}_b(1+\gamma_5)$, leading to the above pattern of relations between the loop amplitudes. We mention that the gluon mass regulator scheme can be converted to the dimensional reduction scheme by the replacement $\log\Lambda^2 \to 1/\epsilon - \gamma_E + \log 4\pi\mu^2/q^2$ where $2\epsilon = 4-N$, γ_E is the Euler-Mascharoni constant $\gamma_E = 0.577\ldots$, and μ is the QCD scale parameter.

VI. TREE GRAPH CONTRIBUTION

The tree graph contribution results from the square of the real gluon emission graphs shown in Figs. 1(c) and 1(d). Omitting again the weak coupling factor $V_{tb}g/\sqrt{2}$ for the time being the corresponding hadron tensor is given by

$$\begin{aligned}\mathcal{H}^{\mu\nu} = -4\pi\alpha_s C_F \frac{8}{(k\cdot p_t)(k\cdot p_b)}\Bigg(&-\frac{k\cdot p_t}{k\cdot p_b}\{(p_b\cdot p_b)(k^\mu \bar{p}_t^\nu + k^\nu \bar{p}_t^\mu - k\cdot\bar{p}_t g^{\mu\nu}) + i[\epsilon^{\alpha\beta\mu\nu}(p_b-k)\cdot\bar{p}_t - \epsilon^{\alpha\beta\gamma\nu}(p_b-k)^\mu \bar{p}_{t,\gamma} \\ &+ \epsilon^{\alpha\beta\gamma\mu}(p_b-k)^\nu \bar{p}_{t,\gamma}]k_\alpha p_{b,\beta}\} + \frac{k\cdot p_b}{k\cdot p_t}\{(\bar{p}_t\cdot p_t)(k^\mu p_b^\nu + k^\nu p_b^\mu - k\cdot p_b g^{\mu\nu} - i\epsilon^{\alpha\beta\mu\nu}k_\alpha p_{b,\beta}) - (\bar{p}_t\cdot k)[(p_t-k)^\mu p_b^\nu \\ &+ (p_t-k)^\nu p_b^\mu - (p_t-k)\cdot p_b g^{\mu\nu} - i\epsilon^{\alpha\beta\mu\nu}(p_t-k)_\alpha p_{b,\beta}]\} - (\bar{p}_t\cdot p_b)(k^\mu p_b^\mu + k^\nu p_b^\mu - k\cdot p_b g^{\mu\nu} - i\epsilon^{\alpha\beta\mu\nu}k_\alpha p_{b,\beta}) \\ &+ (p_t\cdot p_b)(k^\mu\bar{p}_t^\nu + k^\nu\bar{p}_t^\mu - k\cdot\bar{p}_t g^{\mu\nu}) - (k\cdot p_b)(p_t^\mu\bar{p}_t^\nu + p_t^\mu\bar{p}_t^\mu - p_t\cdot\bar{p}_t g^{\mu\nu}) + (k\cdot p_t)[(p_b+k)^\mu\bar{p}_t^\nu + (p_b+k)^\nu\bar{p}_t^\mu \\ &+ (p_b+k)\cdot\bar{p}_t g^{\mu\nu}] + (k\cdot\bar{p}_t)(2p_b^\mu p_b^\nu - p_b\cdot p_b g^{\mu\nu}) - i[\epsilon^{\alpha\beta\mu\nu}(k\cdot\bar{p}_t) + \epsilon^{\alpha\beta\gamma\mu}k^\nu\bar{p}_{t,\gamma} - \epsilon^{\alpha\beta\gamma\nu}k^\mu\bar{p}_{t,\gamma}]p_{b,g\alpha}p_{t,\beta} \\ &+ i[\epsilon^{\alpha\beta\mu\nu}(p_t\cdot\bar{p}_t) + \epsilon^{\alpha\beta\gamma\nu}p_t^\nu\bar{p}_{t,\gamma} - \epsilon^{\alpha\beta\gamma\nu}p_t^\mu\bar{p}_{t,\gamma}]k_\alpha p_{b,\beta}\Bigg) + B^{\mu\nu}\cdot\Delta_{\mathrm{SGF}},\end{aligned} \tag{28}$$

$$\Delta_{\mathrm{SGF}} := -4\pi\alpha_s C_F\left(\frac{m_b^2}{(k\cdot p_b)^2} + \frac{m_t^2}{(k\cdot p_t)^2} - 2\frac{p_b\cdot p_t}{(k\cdot p_b)(k\cdot p_t)}\right), \tag{29}$$

where k is the four-momentum of the emitted gluon. Δ_{SGF} is the IR-divergent *soft gluon function* and $\bar{p}_t = p_t - m_t s_t$ as in Sec. IV.[3]

We have isolated the IR-singular part of the tree graph contribution by splitting off a universal soft gluon factor which multiplies the lowest order Born term tensor $B^{\mu\nu}$. This facilitates the treatment of the soft gluon singularity to be regularized by a (small) gluon mass m_g. Since the soft gluon factor is universal in that it multiplies the lowest order Born contribution, the requisite soft gluon integration has to be done only once and is identical for all eight structure functions. The result for the integrated soft gluon function is given in Sec. VIII. Integrating only the soft gluon function Δ_{SGF} and neglecting the finite part in Eq. (28) amounts to what is called the soft gluon approximation. We emphasize that we always include the full tree graph contribution (soft plus finite part) in our calculation. Also, we integrate over the full phase space of the gluon, and not only up to a given energy cutoff of the gluon.

We have deliberately used a calligraphic notation for the tree graph hadron tensor $\mathcal{H}^{\mu\nu}$ in Eq. (28) since $\mathcal{H}^{\mu\nu}$ is *not* the hadron tensor $H^{\mu\nu}$ defined in Sec. II. In fact, the mass dimension of $\mathcal{H}^{\mu\nu}$ differs from that of $H^{\mu\nu}$. To relate the two

[3]Contrary to the Born term case, here the polarization of the top quark cannot be accounted for by replacing all p_t momenta by their barred counterparts $\bar{p}_t$.

hadron tensors one has to do the appropriate phase space integration on the tree graph hadron tensor.

Next one makes use of the covariant projection operators and the covariant forms of the longitudinal and transverse polarization vectors defined in Sec. II to obtain the contributions to the three unpolarized and five polarized structure functions. Since we are aiming for a fully inclusive measurement regarding the X_b system the resulting expressions have to be integrated over the full two-dimensional phase space. As phase space variables we take the gluon energy k_0 and the W energy q_0 where the k_0 integration is done first. The phase space limits of the respective integrations are given by

$$k_{0,-} \leqslant k_0 \leqslant k_{0,+} \tag{30}$$

and

$$m_W \leqslant q_0 \leqslant \frac{m_t^2 + m_W^2 - (m_b + m_g)^2}{2m_t}, \tag{31}$$

where

$$k_{0,\pm} = \frac{(m_t - q_0)(M_+^2 - 2q_0 m_t) \pm \sqrt{q_0^2 - m_W^2}\sqrt{(M_-^2 - 2q_0 m_t)^2 - 4m_g^2 m_b^2}}{2(m_t^2 + m_W^2 - 2q_0 m_t)} \tag{32}$$

and

$$M_\pm^2 := m_t^2 + m_W^2 - m_b^2 \pm m_g^2. \tag{33}$$

It is clear from Eqs. (30)–(33) that the integration boundaries considerably simplify when the gluon mass is set to zero. In particular, the second square root factor in the $k_{0,\pm}$ boundary turns into a polynomial in q_0 which is an essential simplification for the second q_0 integration. This observation is at the core of our tree level integration strategy exemplified by the partitioned form of Eq. (28). The soft gluon singularity has been isolated and brought into a simple form. The remaining part of the tree graph contribution is IR finite and can be integrated without the gluon mass regulator.

The integration over the gluon energy k_0 ($k_{0,-} \leqslant k_0 \leqslant k_{0,+}$) is simple and the results will not be presented here in explicit analytical form. Instead we present in graphical form in Figs. 4 and 5 some representative results for the differential W-boson energy distribution that result from the real gluon emission graphs Figs. 1(c) and 1(d). Figure 4 shows the W-boson energy distribution for the total rate $d\Gamma_{U+L}/dq_0$. The energy distribution rises sharply from the lower energy limit, where the W boson is produced at rest, then increases rapidly over the intermediate range of W-boson energies, and finally rises sharply again toward the end of the spectrum, where the soft gluon singularity is located. In Fig. 5 we show the same distribution for the partial rate into positive helicity W bosons $d\Gamma_+/dq_0$ [$\Gamma_+ = \frac{1}{2}(\Gamma_U + \Gamma_F)$] for $m_b = 0$ and for $m_b \neq 0$. As mentioned before there is no Born term contribution to $d\Gamma_+/dq_0$ for $m_b = 0$ and thus $d\Gamma_+/dq_0$ possesses no IR singularity in this limit. The absence of the IR singularity in the $m_b = 0$ case (dashed line) is quite apparent in Fig. 5. The distribution rises moderately fast from the lower end of the spectrum, then turns down over the intermediate range of energies, and finally tends to zero at the end of the spectrum where the phase space closes. The $m_b = 0$ (dashed line) and $m_b \neq 0$ (full line) distributions lie on top of each other for most of the lower part of the spectrum. Starting at around 4.8 GeV below the upper phase space boundary the two distributions begin to diverge from each other. Whereas the $m_b = 0$ curve turns down and goes to zero at the end of the spectrum, the $m_b \neq 0$ curve starts to rise again and, in fact, tends to infinity at the end of the spectrum due to its IR-singular behavior. Note the huge differences in scale of the $d\Gamma_{U+L}/dq_0$ and the $d\Gamma_+/dq_0$ distributions which will be reflected in big differences in the total α_s corrections for the two corresponding rates.

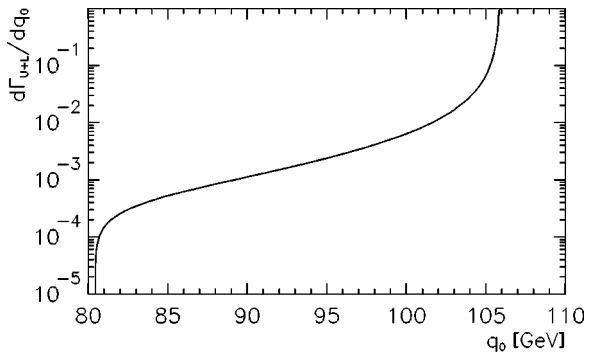

FIG. 4. Differential W-boson energy distribution $d\Gamma_{U+L}/dq_0$ for the total rate resulting from $O(\alpha_s)$ gluon emission ($m_b = 4.8$ GeV).

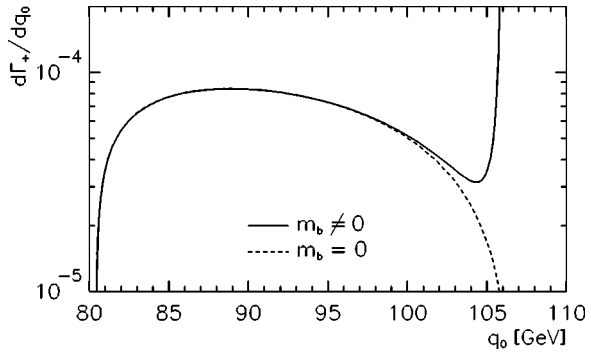

FIG. 5. Differential W-boson energy distribution $d\Gamma_+/dq_0$ for the partial rate into positive helicity W bosons resulting from $O(\alpha_s)$ gluon emission for $m_b = 4.8$ GeV (solid line) and for $m_b = 0$ (dashed line).

The second integration over the energy of the W boson is more difficult. Details can be found in Sec. VIII and in the Appendixes. As it turns out the analytical $m_b \neq 0$ results are quite lengthy. We thus chose to present our $m_b = 0$ results first since they are sufficiently simple to be presented in compact form. They have been obtained by taking the $m_b \to 0$ limit of our $m_b \neq 0$ results written down in Sec. VIII. For practical purposes the $m_b = 0$ results are sufficiently accurate for top-quark decays since $m_b \neq 0$ effects are generally quite small. This is particularly true if a running b-quark mass at the top-quark mass scale is used. Quantitative results for the α_s $m_b \neq 0$ corrections are given at the end of Sec. VIII as well as in [23].

VII. COMPLETE $O(\alpha_s)$ RESULTS FOR $m_b = 0$

We are now in the position to put together our $m_b = 0$ results. We add together the Born term results from Sec. IV, the one-loop results from Sec. V, and the $m_b \to 0$ limit of the integrated tree graph results according to Sec. VIII. The mass and infrared-singular logarithmic terms cancel among the $O(\alpha_s)$ one-loop and tree graph contributions as they must according to the Lee-Nauenberg theorem, and a finite result remains. We choose to present our results in terms of scaled rate functions defined by $\hat{\Gamma}_i := \Gamma_i / \Gamma_0$ $(i = U+L, U^P + L^P, U, L, F, S, U^P, L^P, F^P, S^P, I^P, A^P)$ with $\Gamma_0 = \Gamma_{U+L}(\text{Born})$ given by $(x = m_W/m_t)$

$$\Gamma_0 = \Gamma_{U+L}(\text{Born}) = \frac{G_F m_W^2 m_t}{2\sqrt{2}\pi} |V_{tb}|^2 \frac{(1-x^2)^2(1+2x^2)}{x^2}. \tag{34}$$

The angular decay distribution reads

$$\begin{aligned}
&\frac{d\hat{\Gamma}}{d\cos\theta_P d\cos\theta\, d\phi} \\
&\quad = \frac{1}{4\pi}\left\{ \frac{3}{8}(\hat{\Gamma}_U + P\cos\theta_P \hat{\Gamma}_{U^P})(1+\cos^2\theta) \right. \\
&\qquad + \frac{3}{4}(\hat{\Gamma}_L + P\cos\theta_P \hat{\Gamma}_{L^P})\sin^2\theta \\
&\qquad + \frac{3}{4}(\hat{\Gamma}_F + P\cos\theta_P \hat{\Gamma}_{F^P})\cos\theta \\
&\qquad + \frac{3}{2\sqrt{2}}\hat{\Gamma}_{I^P} P \sin\theta_P \sin 2\theta \cos\phi \\
&\qquad \left. + \frac{3}{\sqrt{2}}\hat{\Gamma}_{A^P} P \sin\theta_P \sin\theta \cos\phi \right),
\end{aligned} \tag{35}$$

where P is the degree of polarization of the top quark. As mentioned before one recovers the angular decay distribution written down in [17] when one substitutes the $m_b = 0$ Born term expressions from Table I in Eq. (35).

The various reduced rates $\hat{\Gamma}_i$ are given by

$$\begin{aligned}
\hat{\Gamma}_{U+L} = 1 + \frac{\alpha_s}{2\pi} C_F \frac{x^2}{(1-x^2)^2(1+2x^2)} \left\{ \frac{(1-x^2)(5+9x^2-6x^4)}{2x^2} - \frac{2(1-x^2)^2(1+2x^2)\pi^2}{3x^2} - \frac{(1-x^2)^2(5+4x^2)}{x^2}\ln(1-x^2) \right. \\
\left. - \frac{4(1-x^2)^2(1+2x^2)}{x^2}\ln(x)\ln(1-x^2) - 4(1+x^2)(1-2x^2)\ln(x) - \frac{4(1-x^2)^2(1+2x^2)}{x^2}\mathrm{Li}_2(x^2) \right\},
\end{aligned} \tag{36}$$

$$\begin{aligned}
\hat{\Gamma}_{(U+L)^P} = \frac{1-2x^2}{1+2x^2} + \frac{\alpha_s}{2\pi} C_F \frac{x^2}{(1-x^2)^2(1+2x^2)} \left\{ -\frac{(1-x)^2(15+2x-5x^2-12x^3+2x^4)}{2x^2} + \frac{(1+4x^2)\pi^2}{3x^2} \right. \\
- \frac{(1-x^2)^2(1-4x^2)}{x^2}\ln(1-x) - \frac{(1-x^2)(3-x^2)(1+4x^2)}{x^2}\ln(1+x) - \frac{4(1-x^2)^2(1-2x^2)}{x^2}\mathrm{Li}_2(x) \\
\left. + \frac{4(2+5x^4-2x^6)}{x^2}\mathrm{Li}_2(-x) \right\},
\end{aligned} \tag{37}$$

$$\begin{aligned}
\hat{\Gamma}_U = \frac{2x^2}{1+2x^2} + \frac{\alpha_s}{2\pi} C_F \frac{x^2}{(1-x^2)^2(1+2x^2)} \left\{ -(1-x^2)(19+x^2) + \frac{2(5+5x^2-2x^4)\pi^2}{3} - 2\frac{(1-x^2)^2(1+2x^2)}{x^2}\ln(1-x^2) \right. \\
- 4(5+7x^2-2x^4)\ln(x) - 2(1-x)^2\frac{(5+7x^2+4x^3)}{x}\ln(x)\ln(1-x) + \frac{2(1-x)^2(5+7x^2-4x^3)}{x}\ln(x)\ln(1+x) \\
\left. - \frac{2(1-x)^2(5+4x+15x^2+8x^3)}{x}\mathrm{Li}_2(x) + \frac{2(1+x)^2(5-4x+15x^2-8x^3)}{x}\mathrm{Li}_2(-x) \right\}
\end{aligned} \tag{38}$$

$$\hat{\Gamma}_L = \frac{1}{1+2x^2} + \frac{\alpha_s}{2\pi} C_F \frac{x^2}{(1-x^2)^2(1+2x^2)} \left\{ \frac{(1-x^2)(5+47x^2-4x^4)}{2x^2} - \frac{2\pi^2}{3}\frac{(1+5x^2+2x^4)}{x^2} - \frac{3(1-x^2)^2}{x^2}\ln(1-x^2) \right.$$
$$+ 16(1+2x^2)\ln(x) - 2(1-x)^2\frac{2-x+6x^2+x^3}{x^2}\ln(1-x)\ln(x) - \frac{2(1+x)^2(2+x+6x^2-x^3)}{x^2}\ln(x)\ln(1+x)$$
$$\left. - \frac{2(1-x)^2(4+3x+8x^2+x^3)}{x^2}\mathrm{Li}_2(x) - \frac{2(1+x)^2(4-3x+8x^2-x^3)}{x^2}\mathrm{Li}_2(-x) \right\}, \tag{39}$$

$$\hat{\Gamma}_F = \frac{-2x^2}{1+2x^2} + \frac{\alpha_s}{2\pi} C_F \frac{x^2}{(1-x^2)^2(1+2x^2)} \left\{ -2(1-x)^2(3-4x) + \frac{2(2+x^2)\pi^2}{3} + \frac{2(1-x^2)^2(1+2x^2)}{x^2}\ln(1-x) \right.$$
$$\left. + \frac{2(1-x^2)(1-9x^2+2x^4)}{x^2}\ln(1+x) + 8(1-x^2)\mathrm{Li}_2(x) + 8(1+3x^2-x^4)\mathrm{Li}_2(-x) \right\}, \tag{40}$$

$$\hat{\Gamma}_S = \frac{1}{1+2x^2} + \frac{\alpha_s}{2\pi} C_F \frac{x^2}{(1-x^2)^2(1+2x^2)} \left\{ \frac{9(1-x^2)^2}{2x^2} - \frac{2(1-x^2)^2\pi^2}{3x^2} + \frac{(1-x^2)^2(2-5x^2)}{x^4}\ln(1-x^2) \right.$$
$$\left. - 4(1-x^2)\ln(x) - \frac{4(1-x^2)^2}{x^2}\ln(x)\ln(1-x^2) - \frac{4(1-x^2)^2}{x^2}\mathrm{Li}_2(x^2) \right\}, \tag{41}$$

$$\hat{\Gamma}_{U^P} = \frac{-2x^2}{1+2x^2} + \frac{\alpha_s}{2\pi} C_F \frac{x^2}{(1-x^2)^2(1+2x^2)} \left\{ -\frac{(1-x)^2(12-55x+6x^2-x^3)}{x} - \frac{10\pi^2}{3}(2+x^2) \right.$$
$$+ \frac{2(1-x^2)^2(1+2x^2)}{x^2}\ln(1-x) + \frac{2(1-x^2)(7+21x^2+2x^4)}{x^2}\ln(1+x) + 8(1-x^2)^2\mathrm{Li}_2(x)$$
$$\left. - 8(11+3x^2+x^4)\mathrm{Li}_2(-x) \right\}, \tag{42}$$

$$\hat{\Gamma}_{L^P} = \frac{1}{1+2x^2} + \frac{\alpha_s}{2\pi} C_F \frac{x^2}{(1-x^2)^2(1+2x^2)} \left\{ -(15-22x+105x^2-24x^3+4x^4)\frac{(1-x)^2}{2x^2} + \frac{(1+24x^2+10x^4)\pi^2}{3x^2} \right.$$
$$\left. - \frac{3(1-x^2)^2}{x^2}\ln(1-x) - \frac{(1-x^2)(17+53x^2)}{x^2}\ln(1+x) - \frac{4(1-x^2)^2}{x^2}\mathrm{Li}_2(x) + \frac{4(2+22x^2+11x^4)}{x^2}\mathrm{Li}_2(-x) \right\}, \tag{43}$$

$$\hat{\Gamma}_{F^P} = \frac{2x^2}{1+2x^2} + \frac{\alpha_s}{2\pi} C_F \frac{x^2}{(1-x^2)^2(1+2x^2)} \left\{ 2(1-x^2)(4+x^2) - \frac{2(1+x^2+2x^4)\pi^2}{3} - \frac{2(1-x^2)^2(1+2x^2)}{x^2}\ln(1-x^2) \right.$$
$$- 4(2-5x^2-2x^4)\ln(x) - \ln(x)\ln(1-x)\frac{4(1-x)^2(1+3x+2x^2+2x^3)}{x}$$
$$+ \frac{4(1+x)^2(1-3x+2x^2-2x^3)}{x}\ln(x)\ln(1+x) - \frac{4(1-x)^2(1+5x+6x^2+4x^3)}{x}\mathrm{Li}_2(x)$$
$$\left. + \frac{4(1+x)^2(1-5x+6x^2-4x^3)}{x}\mathrm{Li}_2(-x) \right\}, \tag{44}$$

$$\hat{\Gamma}_{S^P} = \frac{1}{1+2x^2} + \frac{\alpha_s}{2\pi} C_F \frac{x^2}{(1-x^2)^2(1+2x^2)} \left\{ -\frac{(1-x)^2(11-6x-7x^2)}{2x^2} + \frac{(1+2x^2)\pi^2}{3x^2} + \frac{(1-x^2)^2(2-5x^2)}{x^4}\ln(1-x) \right.$$
$$\left. + \frac{(1-x^2)(2-9x^2+x^4)}{x^4}\ln(1+x) - \frac{4(1-x^2)}{x^2}\mathrm{Li}_2(x) + \frac{4(2+x^4)}{x^2}\mathrm{Li}_2(-x) \right\}, \tag{45}$$

$$\hat{\Gamma}_{I^P}=\frac{-x}{\sqrt{2}(1+2x^2)}+\frac{\alpha_s}{2\pi}C_F\frac{x^2}{(1-x^2)^2(1+2x^2)}\left\{\frac{(1-x)^2(12-7x+12x^2)}{\sqrt{2}x}-\frac{\pi^2}{6\sqrt{2}}\frac{(5+19x^2+2x^4)}{x}\right.$$
$$+\frac{(1-x^2)^2(1+5x^2)}{2\sqrt{2}x^3}\ln(1-x)+\frac{(1-x^2)(1+30x^2+21x^4)}{2\sqrt{2}x^3}\ln(1+x)+\frac{2\sqrt{2}(1-x^2)^2}{x}\mathrm{Li}_2(x)$$
$$\left.-\frac{\sqrt{2}(7+15x^2+4x^4)}{x}\mathrm{Li}_2(-x)\right\}, \tag{46}$$

$$\hat{\Gamma}_{A^P}=\frac{x}{\sqrt{2}(1+2x^2)}+\frac{\alpha_s}{2\pi}C_F\frac{x^2}{(1-x^2)^2(1+2x^2)}\left\{\frac{(1-x^2)(1+2x^2)}{\sqrt{2}x}-\frac{\pi^2}{6\sqrt{2}}\frac{(3-5x^2+6x^4)}{x}-\frac{(1-x^2)^2(1+5x^2)}{2\sqrt{2}x^3}\right.$$
$$\times\ln(1-x^2)-\frac{x(5-11x^2)}{\sqrt{2}}\ln(x)-\frac{(1-x)^2(3+7x+6x^2)}{\sqrt{2}x}\ln(x)\ln(1-x)-\frac{(1+x)^2(3-7x+6x^2)}{\sqrt{2}x}\ln(x)\ln(1+x)$$
$$\left.-\frac{(1-x)^2(7+15x+10x^2)}{\sqrt{2}x}\mathrm{Li}_2(x)-\frac{(1+x)^2(7-15x+10x^2)}{\sqrt{2}}\mathrm{Li}_2(-x)\right\}. \tag{47}$$

As mentioned in the Introduction the results for the total rate $(U+L)$ agree with the analytical results given in [4–7] and in [16]. The six (mass zero) diagonal structure functions U, L, F and U^P, L^P, F^P have already been listed in [16]. They had been checked against the corresponding numerical results given in [27–29]. The results for the nondiagonal structure functions A^P and I^P are new. As for the unpolarized transverse structure functions, explicit expressions for the two linear combinations $T_+=\frac{1}{2}(U+F)$ and $T_-=\frac{1}{2}(U-F)$ relevant for the interpretation of the CDF measurement [1] were given in [23].

We have also included $O(\alpha_s)$ results on the unpolarized and polarized scalar structure functions $\hat{\Gamma}_S$ and $\hat{\Gamma}_{S^P}$. They determine the $m_b=0$ unpolarized and polarized decay of the top quark into a charged Higgs boson $(t\to b+H^+)$ as it occurs, e.g., in the two-Higgs-doublet model (2HDM). This can be seen as follows. The scalar projection of the standard model (SM) left-chiral current structure $\gamma^\mu P_L$ determines the coupling of the SM Goldstone boson, i.e., $\not{q}P_L\to(m_tP_R-m_bP_L)$. This is the coupling structure of the charged Higgs boson in the 2HDM when the ratio of vacuum expectation values is taken to be 1. It is then evident that, for $m_b=0$, the scalar structure functions $\hat{\Gamma}_S$ and $\hat{\Gamma}_{S^P}$ describe the decay $t\to b+H^+$ in the 2HDM, irrespective of the value of the ratio of vacuum expectation values. The unpolarized scalar structure function $\hat{\Gamma}_S$ has been checked against the result of [24]. The result for the polarized scalar structure function $\hat{\Gamma}_{S^P}$ is new.

Before turning to the numerical evaluation of the various contributions we would like to discuss the large m_t limit of the various helicity structure functions. As expected from the statements of the Goldstone boson equivalence theorem the longitudinal and scalar contributions L, L^P, S, and S^P dominate in this limit. In fact, setting $x=0$ one finds

$$\hat{\Gamma}_L=\hat{\Gamma}_S=1+\frac{\alpha_s}{2\pi}C_F\left(\frac{5}{2}-\frac{2}{3}\pi^2\right), \tag{48}$$

$$\hat{\Gamma}_{L^P}=\hat{\Gamma}_{S^P}=1+\frac{\alpha_s}{2\pi}C_F\left(-\frac{15}{2}+\frac{1}{3}\pi^2\right). \tag{49}$$

That $\hat{\Gamma}_L=\hat{\Gamma}_S$ and $\hat{\Gamma}_{L^P}=\hat{\Gamma}_{S^P}$ for $m_t\to\infty$ can be understood from the fact that the longitudinal and scalar polarization vectors $\epsilon^\mu(0)$ and $\epsilon^\mu(S)$ become equal to each other in this limit since the longitudinal polarization vector then simplifies to $\epsilon^\mu(0)=q^\mu/m_W+O(m_W/q_0)$. The same observation is also at the heart of the proof of the Goldstone boson equivalence theorem. As concerns the tree graph contribution, the statement that $\epsilon^\mu(0)=q^\mu/m_W+O(m_W/q_0)$ is certainly not true for all of three-body phase space, e.g., close to the phase space point where the W boson is at rest. The contribution from this phase space region to the three-body rate, however, becomes negligibly small when $m_t\to\infty$.

We now turn to our numerical results. As numerical input values we take $m_t=175$ GeV and $m_W=80.419$ GeV. The strong coupling constant is evolved from $\alpha_s(M_Z)=0.1175$ to $\alpha_s(m_t)=0.1070$ using two-loop running. The results are presented such that the reduced Born term rates are factored out from the reduced rates. This way of presenting the results allows one to quickly assess the size of the radiative corrections. One has

$$\hat{\Gamma}_{U+L}=1-0.0854, \tag{50a}$$

$$\hat{\Gamma}_U=0.297(1-0.0624), \tag{50b}$$

$$\hat{\Gamma}_L=0.703(1-0.0951), \tag{50c}$$

$$\hat{\Gamma}_F=-0.297(1-0.0687), \tag{50d}$$

$$\hat{\Gamma}_{(U+L)^P} = 0.406(1-0.1162), \tag{50e}$$

$$\hat{\Gamma}_{U^P} = -0.297(1-0.0689), \tag{50f}$$

$$\hat{\Gamma}_{L^P} = 0.703(1-0.962), \tag{50g}$$

$$\hat{\Gamma}_{F^P} = 0.297(1-0.0639), \tag{50h}$$

$$\hat{\Gamma}_{I^P} = -0.228(1-0.0810), \tag{50i}$$

$$\hat{\Gamma}_{A^P} = 0.228(1-0.0820), \tag{50j}$$

$$\hat{\Gamma}_S = 0.703(1-0.0895), \tag{50k}$$

$$\hat{\Gamma}_{S^P} = 0.703(1-0.0922). \tag{50l}$$

The radiative corrections to the unpolarized and polarized rate functions are sizable. They range from -6.2% for $\hat{\Gamma}_U$ to -11.6% for $\hat{\Gamma}_{(U+L)^P}$ compared to the rate correction of -8.5%. The radiative corrections to the longitudinal and scalar contributions are the largest. The radiative corrections all tend to go in the same direction. This is an indication that the bulk of the radiative corrections come from phase space regions close to the IR/*M* singular region where the radiative corrections are universal. When normalizing the rate functions to the total rate, as is appropriate for the definition of polarization observables, the size of the radiative corrections to the polarization observables is much reduced. For example, the $O(\alpha_s)$ radiative corrections decrease the ratio Γ_L/Γ_{U+L} by 1.1% and increase the ratio Γ_U/Γ_{U+L} and the magnitude of the ratio Γ_F/Γ_{U+L} by 2.5% and 1.8%, respectively, relative to their Born term ratios. The relative ratio Γ_U/Γ_L is increased by 3.6%. The values of the radiative corrections to the polarization observables are, however, large enough that they must be included in a meaningful comparison of future high precision data with the theoretical predictions of the standard model.

The combination $(\hat{\Gamma}_U+\hat{\Gamma}_F)/2$ determines the decay of an unpolarized top quark into a right-handed *W* boson. This combination vanishes at the Born term level for $m_b=0$ as Eqs. (39) and (41) show. Adding up the corresponding numerical values of the $O(\alpha_s)$ contributions in Eq. (51) one finds that the right-handed *W* boson occurs only with 0.094% probability. The $m_b \neq 0$ effect in the Born term alone already amounts to 0.036% (see Table I).

Altogether the $O(\alpha_s)$ and the Born term $m_b \neq 0$ corrections to the transverse-plus rate occur only at the subpercent level. It is safe to say that, if top-quark decays reveal a violation of the standard model $(V-A)$ current structure that exceeds the 1% level, the violations must have a non-SM origin. In this context it is interesting to note that a possible $(V+A)$ admixture to the SM $t \to b$ current is already severely bounded indirectly to below 5% by existing data on $b \to s+ \to \gamma$ decays [35–37].

The rate combination $(\hat{\Gamma}_U+\hat{\Gamma}_F)/2$ is in fact not the only combination that vanishes at the Born term level for $m_b=0$. Considering the fact that one must have $\lambda_W-\lambda_t=-1/2$ at the Born term level the only surviving Born term level rate expressions are $\hat{\Gamma}^{--}_{--}$, $\hat{\Gamma}^{++}_{00}$, and $\hat{\Gamma}^{-+}_{-0}$ as alluded to before in Sec. IV. The notation employed for the reduced rates follows the notation used in Eq. (13a). The remaining rate expressions vanish at the Born term level but become populated at $O(\alpha_s)$. They are

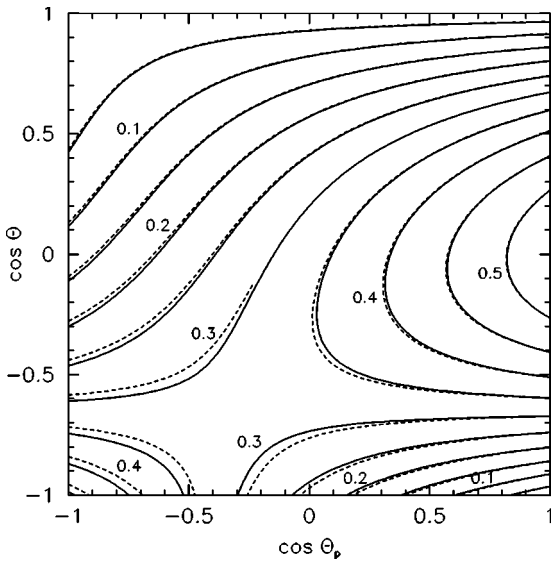

FIG. 6. Contours of the decay distribution of a fully polarized $(P=1)$ top quark in the $\cos\theta_P$-$\cos\theta$ plane for $m_b=0$. The full lines are the distribution including the $O(\alpha_s)$ corrections.

$$\hat{\Gamma}^{++}_{++} = \tfrac{1}{4}(\hat{\Gamma}_U+\hat{\Gamma}_F+\hat{\Gamma}_{U^P}+\hat{\Gamma}_{F^P}) = 0.000\,833,$$

$$\hat{\Gamma}^{--}_{00} = \tfrac{1}{2}(\hat{\Gamma}_L-\hat{\Gamma}_{L^P}) = 0.000\,289,$$

$$\hat{\Gamma}^{+-}_{+0} = (\hat{\Gamma}_{I^P}+\hat{\Gamma}_{A^P}) = -0.000\,236, \tag{51}$$

$$\hat{\Gamma}^{--}_{++} = \tfrac{1}{4}(\hat{\Gamma}_U+\hat{\Gamma}_F-\hat{\Gamma}_{U^P}-\hat{\Gamma}_{F^P}) = 0.000\,093,$$

$$\hat{\Gamma}^{++}_{--} = \tfrac{1}{4}(\hat{\Gamma}_U-\hat{\Gamma}_F+\hat{\Gamma}_{U^P}-\hat{\Gamma}_{F^P}) = 0.000\,120.$$

As remarked on before the last two reduced rates $\hat{\Gamma}^{--}_{++}$ and $\hat{\Gamma}^{++}_{--}$ vanish at the Born term level even for $m_b \neq 0$ since the net helicity of these transitions $|\lambda_W-\lambda_t|=3/2$ exceeds that of the *b* quark $|\lambda_b|=1/2$.

The four reduced rates $\hat{\Gamma}^{++}_{++}$, $\hat{\Gamma}^{--}_{00}$, $\hat{\Gamma}^{--}_{++}$, and $\hat{\Gamma}^{++}_{--}$ are positive definite quantities since they result from squares of helicity amplitudes. Contrary to these, $\hat{\Gamma}^{+-}_{+0}$ is an interference contribution and thus can be negative, as it in fact is. In Eq. (51) we have also included the numerical values for the above five structure function combinations resulting from the (tree graph) α_s corrections. They are all very small at the levels lower than parts per thousand.

In Sec. IV (Fig. 3) we have shown a Lego plot of the Born term twofold angular decay distribution in $\cos\theta$ and $\cos\theta_P$. In order to be able to exhibit the size of the α_s corrections we show in Fig. 6 a contour plot of the same twofold angular decay distribution with and without radiative corrections,

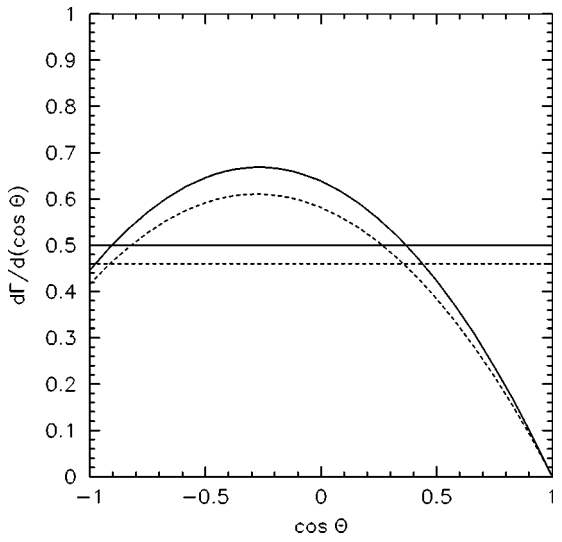

FIG. 7. Charged lepton polar angular distribution in the W rest frame for $m_b=0$ [Born term, full line; $O(\alpha_s)$, dashed line]. Also shown are average values of the decay distribution.

again setting $P=1$. The radiative corrections are not very large in the upper two quadrants and become largest in the lower left quadrant of the contour plot when both $\cos\theta$ and $\cos\theta_P$ tend to 1.

Instead of analyzing the threefold or twofold angular decay distributions one can also consider single angle decay distributions. They are obtained by integrating over the two respective complementary decay angles. For the $\cos\theta$ distribution one obtains

$$\frac{d\hat{\Gamma}}{d\cos\theta}=\tfrac{3}{8}(\hat{\Gamma}_U+2\hat{\Gamma}_L)(1-\alpha_\theta\cos\theta+\beta_\theta\cos^2\theta), \quad (52)$$

where

$$\alpha_\theta=2\frac{\hat{\Gamma}_F}{\hat{\Gamma}_U+2\hat{\Gamma}_L}\quad\left(=-\frac{2x^2}{1+x^2}=-0.349\right), \quad (53)$$

$$\beta_\theta=\frac{\hat{\Gamma}_U-2\hat{\Gamma}_L}{\hat{\Gamma}_U+2\hat{\Gamma}_L}\quad\left(=-\frac{1-x^2}{1+x^2}=-0.651\right). \quad (54)$$

We have added the analytical and numerical Born term results for the asymmetry parameters in parentheses using $x^2=0.211$. The $O(\alpha_s)$ values for the asymmetry parameters are $\alpha_\theta=-0.357$ and $\beta_\theta=-0.641$, i.e., the α_s corrections raise the magnitude of α_θ by 2.3% and lower the magnitude of β_θ by 1.5%. In Fig. 7 we show the $\cos\theta$ distribution for both the Born term case and the radiatively corrected case. There is a pronounced forward-backward asymmetry. In the forward direction the differential Born term rate drops to zero. As discussed before the $O(\alpha_s)$ rate does not vanish in the forward direction due to real gluon emission. However, the radiative corrections are so small that the nonvanishing of the $O(\alpha_s)$ rate in the forward direction cannot be discerned at the scale of the plot. In absolute terms the radiative corrections are largest for $\cos\theta\approx 0$ because of the large size of the radiative corrections to the longitudinal rate $\hat{\Gamma}_L$. Note that α_θ is not the conventional forward-backward asymmetry parameter, which is defined by

$$\alpha_{\rm FB}=\frac{d\Gamma(0\geqslant\theta\geqslant\pi/2)-d\Gamma(\pi/2\geqslant\theta\geqslant\pi)}{d\Gamma(0\geqslant\theta\geqslant\pi/2)+d\Gamma(\pi/2\geqslant\theta\geqslant\pi)}$$
$$=\frac{3}{4}\frac{\hat{\Gamma}_F}{\hat{\Gamma}_{U+L}}\quad\left(=-\frac{3}{2}\frac{x^2}{1+2x^2}=-0.223\right). \quad (55)$$

The α_s corrections raise $\alpha_{\rm FB}$ by 1.7% in magnitude.

For the $\cos\theta_P$ distribution one obtains

$$\frac{d\hat{\Gamma}}{d\cos\theta_P}=\frac{1}{2}(\hat{\Gamma}_{U+L})(1+P\alpha_{\theta_P}\cos\theta_P), \quad (56)$$

where

$$\alpha_{\theta_P}=\frac{\hat{\Gamma}_{(U+L)^P}}{\hat{\Gamma}_{U+L}}\quad\left(=\frac{1-2x^2}{1+2x^2}=0.406\right). \quad (57)$$

The α_s corrections lower α_{θ_P} by 3.4%.

Finally, the ϕ distribution reads

$$\frac{d\hat{\Gamma}}{d\phi}=\frac{1}{2\pi}(1+P\gamma_\phi\cos\phi), \quad (58)$$

where

$$\gamma_\phi=\frac{3\pi^2}{8\sqrt{2}}\frac{\hat{\Gamma}_{A^P}}{\hat{\Gamma}_{U+L}}\quad\left(=\frac{3\pi^2}{16}\frac{x}{1+2x^2}=0.597\right). \quad (59)$$

The $\cos\phi$ dependent contribution from $\hat{\Gamma}_{I_P}$ has dropped out because of having integrated over the full range of $\cos\theta$. If desired, the contribution of $\hat{\Gamma}_{I_P}$ to the ϕ distribution can be retained if one integrates only over half the range of $\cos\theta$. The α_s corrections raise γ_ϕ by the small amount of 0.32%. In Fig. 8 we show the ϕ distribution for both the Born term case and the radiatively corrected case, setting $P=1$.

VIII. COMPLETE $O(\alpha_s)$ RESULTS FOR $m_b\neq 0$

Differing from the presentation of our $m_b=0$ results in Sec. VII, we shall present our $m_b\neq 0$ results in a form where each of the separate contributions to the rate remains identified. In particular, we do not explicitly cancel the IR terms coming from the one-loop and tree graph contributions. We thus write

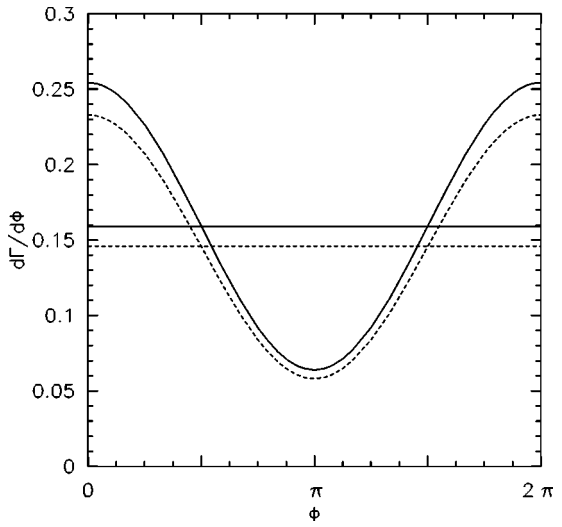

FIG. 8. Azimuthal distribution of normalized rate for $m_b=0$ [Born term, full line; $O(\alpha_s)$, dashed line]. Also shown are average values of the decay distribution.

$$\Gamma_i^{\rm QCD}=\Gamma_i({\rm Born})+\frac{m_t^3|V_{tb}|^2G_F}{8\sqrt{2}\pi}\left\{\sum_\tau\ \kappa_{i,\tau}F_\tau\right\}$$
$$+\frac{4}{\sqrt{\lambda}}\Gamma_i({\rm Born})S(\Lambda)-\frac{\alpha_s}{4\pi}\frac{m_t^3|V_{tb}|^2G_Fx^2}{8\sqrt{2}\pi}$$
$$\times\left\{\sum_{n=-1,0}\rho_{(n),i}\mathcal{R}_{(n)}+\sum_{m,n}\rho_{(m,n),i}\mathcal{R}_{(m,n)}\right.$$
$$\left.+\sum_{n=0,1}\sigma_{(n),i}\mathcal{S}_{(n)}+\sum_{m,n}\sigma_{(m,n),i}\mathcal{S}_{(m,n)}\right\}. \qquad (60)$$

The first term in Eq. (60) represents the Born term contribution, which is given by

$$\Gamma_i({\rm Born})=\frac{G_Fm_W^2|V_{tb}|^2}{8\sqrt{2}\pi m_t}\sqrt{\lambda}B_i \qquad (61)$$

where the B_i are the Born term rates listed in Table I. The Born term contribution Γ_i(Born) also appears as a factor in the third term where it multiplies the soft gluon factor $S(\Lambda)$. The index i runs over the various structure function labels $i=U+L$, U^P+L^P, U, U^P, L, L^P, F, F^P, S, S^P, I^P, and A^P.

The second term in Eq. (60) represents the one-loop contribution which is obtained by folding the one-loop amplitude in Appendix C with the Born term amplitude and then doing the appropriate projection onto the various structure functions. The appropriate coefficient functions $\kappa_{i,\tau}$ are listed in Table II. The coefficient functions $\kappa_{i,\tau}$ multiply the α_s one-loop amplitudes $F_\tau=F_1^V,F_2^V,F_3^V,F_1^A,F_2^A,F_3^A$ which are listed in Appendix C. We label the one-loop amplitudes consecutively by the index $\tau=1,...,6$. Note that Table II contains only the vector current coefficient functions $\kappa_{i,\tau}$ ($\tau=1,2,3$). The axial vector coefficient functions labeled by $\tau=4,5,6$, can be easily obtained from the vector current coefficient functions by the substitution

$$\kappa_{F_1^A}=\kappa_{F_1^V}|_{yu\to -y}\,,\quad \kappa_{F_2^A}=-\kappa_{F_2^V}|_{y\to -y}\,,$$
$$\kappa_{F_3^A}=-\kappa_{F_3^V}|_{y\to -y}\,. \qquad (62)$$

The third term in Eq. (60) contains the result of integrating the soft gluon function $\Delta_{\rm SGF}$ in Eq. (28). The result depends on the (small) IR regularization parameter $\Lambda=m_g/m_t$ as indicated in the argument of the soft gluon factor $S(\Lambda)$. The universal soft gluon factor $S(\Lambda)$ is obtained by explicit integration and reads

TABLE II. Coefficient functions $\kappa_{i,\tau}$ that determine the contributions of the α_s vector current one-loop amplitudes to the different rates Γ_i ($x=m_W/m_t$, $y=m_b/m_t$, $\lambda=1+x^4+y^4-2x^2y^2-2x^2-2y^2$).

i	$\kappa_{F_1^V},i$	$\kappa_{F_2^V},i$	$\kappa_{F_3^V},i$
$U+L$	$\sqrt{\lambda}[(1-y)^2-x^2][(1+y)^2+2x^2]$	$(1/2)m_t\sqrt{\lambda^3}(1+y)$	$(1/2)m_t\sqrt{\lambda^3}(1+y)$
U^P+L^P	$\lambda(1-2x^2-y^2)$	$(1/2)m_t\lambda[(1+y)^2-x^2](1-y)$	$(1/2)m_t\lambda[(1+y)^2-x^2](1-y)$
U	$2\sqrt{\lambda}[(1-y)^2-x^2]x^2$	0	0
U^P	$-x^2\lambda$	0	0
L	$\sqrt{\lambda}[(1-y)^2-x^2](1+y)^2$	$(1/2)m_t\sqrt{\lambda^3}(1+y)$	$(1/2)m_t\sqrt{\lambda^3}(1+y)$
L^P	$\lambda(1-y^2)$	$(1/2)m_t\lambda[(1+y)^2-x^2]^2(1-y)$	$(1/2)m_t\lambda[(1+y)^2-x^2]^2(1-y)$
F	$-2\lambda x^2$	0	0
F^P	$2\sqrt{\lambda}[(1-y)^2-x^2]x^2$	0	0
S	$\sqrt{\lambda}[(1+y)^2-x^2](1-y)^2$	$(1/2)m_t\sqrt{\lambda}[(1+y)^2-x^2]$ $\times(1+x^2-y^2)(1-y)$	$(1/2)m_t\sqrt{\lambda}[(1+y)^2-x^2]$ $\times(1-x^2-y^2)(1-y)$
S^P	$\lambda(1-y^2)$	$(1/2)m_t\lambda(1+x^2-y^2)(1+y)$	$(1/2)m_t\lambda(1-x^2-y^2)(1+y)$
I^P	$-(1/\sqrt{2})\lambda x$	$(1/4\sqrt{2})m_t\lambda[(1+y)^2-x^2]x$	$-(1/4\sqrt{2})m_t\lambda[(1+y)^2-x^2]x$
A^P	$(1/\sqrt{2})\sqrt{\lambda}[(1-y)^2-x^2](1+y)x$	$(1/4\sqrt{2})m_t\sqrt{\lambda^3}x$	$(1/4\sqrt{2})m_t\sqrt{\lambda^3}x$

TABLE III. Range of values of powers m, n in the different basic tree graph integrals.

i	$\rho_{(n),i}$	$\rho_{(m,n),i}$	$\sigma_{(n),i}$	$\sigma_{(m,n),i}$
$U+L$	—	$(-2,-1)$–$(0,-1)$	—	$(0,0)$, $(1,0)$
U^P+L^P	$-1,0$	$(-2,0)$–$(1,0)$	$0,1$	$(0,0)$, $(0,1)$–$(2,1)$
U	—	$(-2,1)$–$(2,1)$	—	$(0,2)$–$(3,2)$
U^P	$-1,0$	$(-2,2)$–$(3,2)$	$0,1$	$(0,0)$, $(0,3)$–$(4,3)$
L	—	$(-2,1)$–$(2,1)$	—	$(0,2)$–$(3,2)$
L^P	$-1,0$	$(-2,2)$–$(3,2)$	$0,1$	$(0,0)$, $(0,3)$–$(4,3)$
F	$-1,0$	$(-2,0)$–$(1,0)$	$0,1$	$(0,0)$, $(0,1)$–$(2,1)$
F^P	—	$(-2,1)$–$(2,1)$	—	$(0,2)$–$(3,2)$
S	—	$(-2,-1)$–$(0,-1)$	—	$(0,0)$–$(1,0)$
S^P	$-1,0$	$(-2,0)$–$(1,0)$	$0,1$	$(0,0)$, $(0,1)$–$(2,1)$
I^P	$-1,0$	$(-2,2)$–$(2,2)$	$0,1$	$(0,0)$, $(0,3)$–$(3,3)$
A^P	—	$(-2,1)$–$(1,1)$	—	$(0,2)$–$(2,2)$

$$S(\Lambda)=-\frac{\alpha_s}{4\pi}C_F\Bigg((1-x^2+y^2)\Bigg\{2\,\mathrm{Li}_2(1-w_1w_\mu)+\mathrm{Li}_2(1-w_1^2)-\mathrm{Li}_2\left(1-\frac{w_1}{w_\mu}\right)+\frac{1}{4}\ln^2(w_1w_\mu)+\ln(w_1w_\mu)\left[\ln\left(\frac{\lambda w_1}{xy\Lambda}\right)+\frac{1}{2}\right]\Bigg\}+2\sqrt{\lambda}\left[\ln\left(\frac{\lambda}{xy\Lambda}\right)-2\right]+\ln\left(\frac{w_1}{w_\mu}\right)-2y^2\ln(w_1)\Bigg), \tag{63}$$

where as in [3] we have used the abbreviations

$$w_1=\frac{x}{y}\cdot\frac{1-x^2+y^2-\sqrt{\lambda}}{1+x^2-y^2+\sqrt{\lambda}},\quad w_\mu=\frac{x}{y}\cdot\frac{1-x^2+y^2-\sqrt{\lambda}}{1+x^2-y^2-\sqrt{\lambda}}. \tag{64}$$

In the limit $y\to 0$ one has

$$S(\Lambda)=-\frac{\alpha_s}{4\pi}C_F\Bigg\{(1-x^2)\left[\frac{\pi^2}{3}-4+\ln^2 y-2\ln\Lambda+(1+2\ln\Lambda)\ln\left(\frac{1-x^2}{y}\right)-2\ln\left(\frac{x}{1-x^2}\right)+\ln(1-x^2)\ln\left(\frac{x^2}{1-x^2}\right)+\mathrm{Li}_2(x^2)\right]+\ln x^2\Bigg\}. \tag{65}$$

In agreement with the Lee-Nauenberg theorem the logarithmic dependence on the IR regularization parameter Λ can be seen to cancel between the loop and the soft gluon contributions for each of the ten structure functions.

The fourth term in Eq. (60) finally contains the result of integrating the finite piece in the tree graph contribution Eq. (28), again after having done the appropriate projections. The result is given in terms of a set of standard integrals $\mathcal{R}_{(n)}$, $\mathcal{R}_{(m,n)}$, $\mathcal{S}_{(n)}$, and $\mathcal{S}_{(m,n)}$ which are listed in Appendix A. Appendix B gives the values of the coefficient functions $\rho_{(n),i}$, $\rho_{(m,n),i}$, $\sigma_{(n),i}$, and $\sigma_{(m,n),i}$ that multiply the standard set of integrals in the various helicity structure functions. In Table III we have listed the range of values of the parameters m and n that characterize the different types of tree graph integrals.

At this point it is perhaps appropriate to offer an excuse to the potential user of our $m_b\neq 0$ results that our results are presented in a multiply nested form to be collected from Eqs. (60)–(64), Table II, and Appendixes A, B, and C. Contrary to the $m_b=0$ results where a closed form representation was possible, a presentation of unnested closed form expressions for $m_b\neq 0$ would require an extraordinary amount of space because of the presence of many different logarithmic and dilogarithmic functions and products thereof. Codes of the relevant expressions can be obtained from the authors on request.

When we evaluated Eq. (60) numerically the IR factors proportional to $\ln\Lambda$ in the one-loop and tree graph contributions were set to zero by hand. The numerical evaluation of the remaining part is quite stable numerically. In particular, the limit $m_b\to 0$ is numerically quite smooth. This is demonstrated in Fig. 9 where we plot the bottom-quark mass dependence of the total rate. Note that the $O(\alpha_s)$ rate shows less dependence on the bottom-quark mass than does the Born term rate.

The quality of the $m_b=0$ approximation has been discussed before at the Born level. For example, at the Born term level the total rate is decreased by 0.27% when going from $m_b=0$ to $m_b=4.8$ GeV. Using the $O(\alpha_s)$ $m_b\neq 0$ results from this section one finds that the $m_b\neq 0$ corrections to the total $O(\alpha_s)$ rate reduce the rate by 0.16% compared to the Born term reduction of 0.27%, i.e., the $m_b\neq 0$ corrections to the α_s contribution alone tend to counteract the $m_b\neq 0$ effect in the Born term in the total rate (see also Fig. 9). The $m_b\neq 0$ corrections from the α_s contributions alone are surprisingly large considering the fact that the factor multiplying the α_s corrections, $C_F\alpha_s/(2\pi)=0.023$, is a rather small number. This can be understood in part by noting that the α_s contributions contain terms proportional to $(m_b^2/m_W^2)\ln(m_b^2/m_t^2)=-0.026$ which is not a very small number. A further discussion of $m_b\neq 0$ effects for the α_s contributions can be found in [23]. Noteworthy is a large 20%

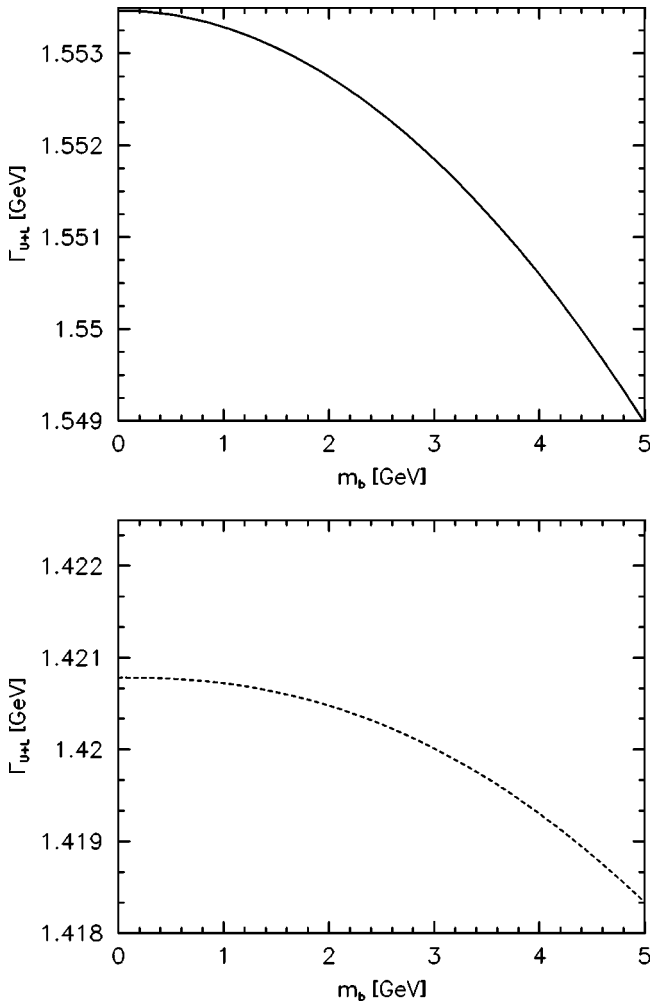

FIG. 9. Bottom-quark mass dependence of the total rate Γ_{U+L} [Born term, full line; $O(\alpha_s)$, dashed line].

correction to the $O(\alpha_s)$ transverse-plus rate $\hat{\Gamma}_+$ due to m_b effects [23]. That the bottom-quark mass effect is so large in $\hat{\Gamma}_+$ can be appreciated in part by looking at the differential distribution in Fig. 5. We emphasize again that the mass effect may have been overestimated due to using a fixed pole mass, rather than a running mass, which is smaller at the top-quark mass scale.

IX. SUMMARY AND CONCLUSION

We have obtained analytical expressions for the $O(\alpha_s)$ radiative corrections to the three unpolarized and five polarized structure functions that govern the decay of a polarized top quark. Although bottom-quark mass effects are quite small in top-quark decays we have retained the full bottom-mass dependence in our calculation. In the limit $m_b \to 0$ the analytical results considerably simplify, leading to compact expressions for the eight structure functions that are listed in the main text. The full mass dependence of our analytical results is written down in Sec. VIII and in the Appendixes A and B. These finite mass results will prove useful for the theoretical description of $b \to c$ bottom-meson and bottom-baryon decays (see, e.g., [38]).

For top-quark decays the radiative corrections to the structure functions range from -6.2% to -11.6% where the radiative corrections to the unpolarized longitudinal structure functions $\hat{\Gamma}_L$ and the polarized structure function $\hat{\Gamma}_{(U+L)^P}$ are largest. These corrections are to be compared with the correction to the total rate, which is -8.5%. The radiative corrections to the structure functions all go in the same directions indicating that the bulk of the radiative corrections derive from contributions close to the IR or M region of phase space where the radiative corrections are universal. Nevertheless, the span of values of the radiative corrections exceeds 5% and must be taken into account in a future comparison with precision experiments. The radiative corrections to rate combinations that vanish at the Born term level have been found to be rather small. In particular, the α_s correction to the normalized rate of an unpolarized top-quark decay into positive helicity W bosons amounts to only 0.1%. As discussed in Sec. VII, the minuteness of the α_s contribution to positive helicity W bosons is of relevance when discussing a possible $(V+A)$ admixture to the standard model current.

We have also determined the $O(\alpha_s)$ corrections to unpolarized and polarized $q_1 \to q_2$ scalar current transitions. For $t \to b$ transitions these scalar current transitions are relevant for top-quark decays into a bottom quark and a charged Higgs boson as they occur in the two-Higgs-doublet model. For $b \to c$ transitions these transition matrix elements are needed, e.g., for the description of the semi-inclusive decays of the B mesons and the Λ_b into spin zero D_s mesons [38,39].

In this paper we have studied only the first order QCD corrections to the structure functions in polarized top-quark decays. For the total rate one obtains a correction of -8.5%. Second order QCD corrections to the rate are expected to amount to -2.6% [40] while electroweak corrections are known to increase the rate by $+1.7\%$ [3,41]. For a high precision comparison of theory and experiment of the structure functions it would therefore be desirable to calculate the two-loop $O(\alpha_s^2)$ and the electroweak one-loop corrections to the eight structure functions. While the two-loop QCD corrections to the structure functions are very difficult and are therefore not likely to be done in the next few years, calculation of the one-loop electroweak corrections to the eight structure functions is presently under way [25]. Finite width corrections will also have to be accounted for. They lower the total width by 1.56% [25,26] and affect the different partial helicity rates by differing amounts [25].

We would like to conclude this paper with a speculative note concerning a possible top-quark mass measurement from an angular decay analysis using the fact that the structure functions are top-quark mass dependent. This suggestion is much in the spirit of the suggestion of Grunberg *et al.*, who advocated a similar measurement of heavy quark masses in the context of e^+e^- annihilations [42]. Assume that the percentage measurement errors on an $L/(U+L)$ and $U/(U+L)$ measurement are δ_L and δ_U, respectively. The percentage error on the mass measurement will be denoted by δ, i.e., we write $m_t = \overline{m}_t(1 \pm \delta)$ where $\overline{m}_t$ is some given

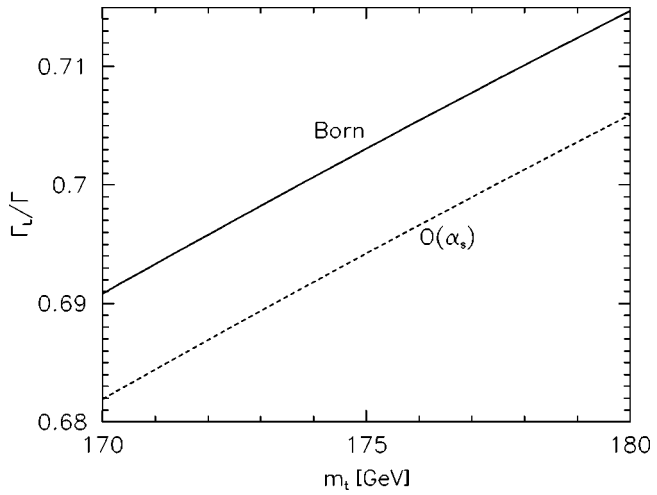

FIG. 10. Top-quark mass dependence of the rate ratio Γ_L/Γ_{U+L} for $m_b=0$ [Born term, full line; $O(\alpha_s)$, dashed line].

central value of the top-quark mass. From the dependence of the respective Born term ratios on the mass ratio $x=m_W/m_t$ (assuming that the W mass is fixed) one finds that the percentage error on the top-quark mass measurement is given by $\delta=\delta_L(1+2x_0^2)/(4x_0^2)$ and by $\delta=\delta_U(1+2x_0^2)/2$, respectively, where we write $x^2=x_0^2(1\mp 2\delta)$ with $x_0=m_W/\overline{m_t}$. If we take $m_t=175$ GeV as the central value ($x_0^2=0.211$) this would imply that a 1% error on the angular structure function measurement would allow one to determine the top-quark mass with 1.7% and 0.7% accuracy, depending on whether the angular measurement was done on the longitudinal (L) or on the unpolarized transverse (U) [or for that matter on the (F)] mode. Since the radiative corrections change the ratios Γ_L/Γ_{U+L} and Γ_U/Γ_{U+L} by 1.1% and 2.4%, respectively, it is clear that one has to use the full $O(\alpha_s)$ results for the angular structure functions if such experimental accuracies can be reached. This is illustrated in Figs. 10 and 11 where we plot the top-quark mass dependence of Γ_L/Γ_{U+L} and Γ_U/Γ_{U+L} for the Born term case and the $O(\alpha_s)$ case for $m_b=0$. Note that the $O(\alpha_s)$ curves are horizontally displaced from the Born term curves by approximately 3 and 3.4 GeV, respectively, meaning that one would make the corresponding mistakes in the top-quark mass determination from a measurement of the angular structure functions if the Born curves were used instead of the radiatively corrected ones. The present Tevatron run I uncertainties on the top-quark mass are around 4%, which is anticipated to be improved to 1.7% during the initial stages of Tevatron run II. It remains to be seen whether a mass determination based on angular measurements as proposed here can compete with the conventional method using invariant mass reconstruction.

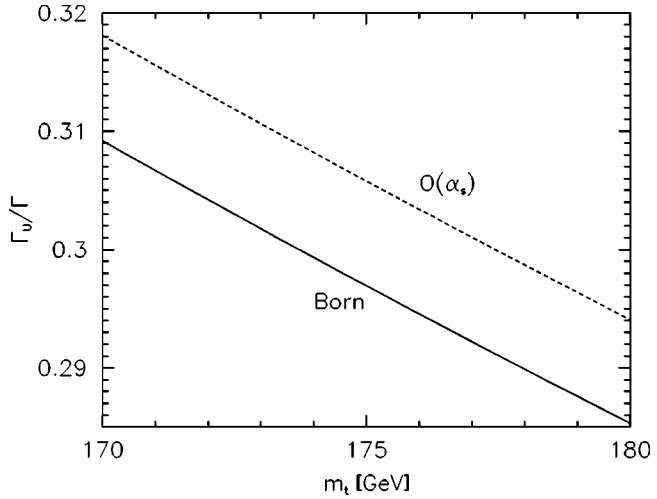

FIG. 11. Top-quark mass dependence of the rate ratio Γ_U/Γ_{U+L} for $m_b=0$ [Born term, full line; $O(\alpha_s)$, dashed line].

ACKNOWLEDGMENTS

M.F. and M.C.M. were partly supported by the DFG (Germany) through the Graduiertenkolleg ''Teilchenphysik bei hohen und mittleren Energien'' and its successor ''Eichtheorien'' at the University of Mainz. M.C.M. was also supported by the BMBF (Germany) under contract 05HT9UMB/4 S.G. and J.G.K. acknowledge partial support by the BMBF (Germany) under contract 06MZ865 and S.G. acknowledges support by the DFG. We would like to thank B. Lampe for initial participation in the project, H. Spiesberger for illuminating discussions, and A. Arbuzov for checking some of the formulas.

APPENDIX A: INTEGRALS

In this appendix we catalog the basic set of tree graph integrals that are needed in our $m_b\neq 0$ calculation and give their analytical results.

1. Basic integrals

In the first step of the tree graph integration one integrates over the gluon energy k_0. After having done the integration on the gluon energy it proves to be convenient to perform a shift in the W energy q_0 integration variable by introducing the variable $z=1+x^2-2q_0/m_t$. One then encounters the following set of integrals:

$$\mathcal{R}_{(m,n)} := \int_{y^2+\epsilon_2'}^{(1-x)^2-\epsilon_1'} \frac{z^m dz}{\sqrt{\lambda^n(1,x^2,z)}},$$

$$\mathcal{R}_{(n)} := \int_{y^2+\epsilon_2'}^{(1-x)^2-\epsilon_1'} \frac{dz}{(z-y^2)\sqrt{\lambda^n(1,x^2,z)}}, \tag{A1a}$$

$$\mathcal{S}_{(m,n)} := \int_{y^2+\epsilon_2'}^{(1-x)^2-\epsilon_1'} \frac{z^m dz}{\sqrt{\lambda^n(1,x^2,z)}} \times \ln\left(\frac{1-x^2+z+\sqrt{\lambda(1,x^2,z)}}{1-x^2+z-\sqrt{\lambda(1,x^2,z)}}\right), \tag{A1b}$$

$$\mathcal{S}_{(n)} := \int_{y^2+\epsilon_2'}^{(1-x)^2-\epsilon_1'} \frac{dz}{(z-y^2)\sqrt{\lambda^n(1,x^2,z)}} \times \ln\left(\frac{1-x^2+z+\sqrt{\lambda(1,x^2,z)}}{1-x^2+z-\sqrt{\lambda(1,x^2,z)}}\right), \tag{A1c}$$

where $\lambda(1,x^2,z)=1+x^4+z^2-2x^2z-2x^2-2z$. The required ranges of values of the parameters m and n are listed in Table III. The cutoff parameters ϵ_1' and ϵ_2' are needed to account for the spurious singularities that are artificially introduced by partial fractioning the integrands. The spurious singularities cancel as they must when all contributions to a particular helicity structure function are summed.

In order to get rid of the square roots the final substitution $z := 1+x^2-x(r+1)/r$ is introduced. The variable r has to be integrated in the interval $[1+\epsilon_1, \eta-\epsilon_2]$, where

$$\eta=(1+x^2-y^2+\sqrt{\lambda})/2x \quad \text{and} \quad \lambda=\lambda(1,x^2,y^2) \tag{A2}$$

as before. The spurious cutoff parameters ϵ_1 and ϵ_2 replace the above cutoff parameters ϵ_1' and ϵ_2' and cancel in all final expressions.

In order to keep our results at a manageable length we introduce the following set of auxiliary functions:

$$\mathcal{L}_1 := \ln\left(\frac{\eta-x}{\eta(1-\eta x)}\right), \quad \mathcal{L}_2 := \ln\left(\frac{\eta(\eta-x)}{1-\eta x}\right), \tag{A3a}$$

$$\mathcal{L}_3 := \ln\left(\frac{(1-x)^2-y^2}{x}\,\frac{(1-x)^2}{\epsilon_1^2 y^2}\right),$$

$$\mathcal{L}_4 := \ln\left(\frac{(1+x)^2-y^2}{x}\,\frac{(1-x)^2}{4y^2}\right), \tag{A3b}$$

$$\mathcal{L}_5 := \ln\left(\frac{1-x}{y}\right), \quad \mathcal{L}_6 := \ln\left(\frac{\eta(1-x)}{\eta-x}\right), \tag{A3c}$$

$$\mathcal{N}_0 := \mathrm{Li}_2(\eta x) + \mathrm{Li}_2\left(\frac{x}{\eta}\right) - 2\,\mathrm{Li}_2(x), \tag{A3d}$$

$$\mathcal{N}_1 := \mathrm{Li}_2(\eta x) - \mathrm{Li}_2\left(\frac{x}{\eta}\right),$$

$$\mathcal{N}_2 := -\ln(\eta)\ln(1+x) + \ln\left(\frac{\eta-x}{(\eta-1)(1+x)}\right)\ln\left(\frac{\eta-x}{\eta(1-\eta x)}\right) - \mathrm{Li}_2\left(\frac{1}{\eta}\right) + \mathrm{Li}_2\left(\frac{(\eta^2-1)x}{\eta-x}\right) + \mathrm{Li}_2\left(\frac{1-\eta x}{\eta-x}\right), \tag{A3e}$$

$$\mathcal{N}_3 := -\ln(\eta)\ln(1-x) - \ln\left(\frac{(\eta+1)(1-x)}{\eta-x}\right)\ln\left(\frac{\eta-x}{\eta(1-\eta x)}\right) - \mathrm{Li}_2\left(-\frac{1}{\eta}\right) + \mathrm{Li}_2\left(\frac{(\eta^2-1)x}{\eta-x}\right) + \mathrm{Li}_2\left(-\frac{1-\eta x}{\eta-x}\right), \tag{A3f}$$

and

$$\beta_+(n) := (x-1)^n + (x+1)^n, \quad \beta_-(n) := (x-1)^n - (x+1)^n, \tag{A3g}$$

$$\beta(n) := \frac{(x-1)^n}{\eta-1} - \frac{(1+x)^n}{\eta+1}. \tag{A3h}$$

In the following we list our analytical results for the various types of integrals that are needed in our calculation.

2. Integrals of type $\mathcal{R}_{(m,n)}$

$$\mathcal{R}_{(-2,-1)} = \frac{\lambda^{1/2}}{y^2} + \frac{\mathcal{L}_2-\mathcal{L}_1}{2} - \frac{1+x^2}{1-x^2}\,\frac{\mathcal{L}_2+\mathcal{L}_1}{2}, \tag{A4a}$$

$$\mathcal{R}_{(-1,-1)} = -\lambda^{1/2} - (1+x^2)\,\frac{\mathcal{L}_2-\mathcal{L}_1}{2} + (1-x^2)\,\frac{\mathcal{L}_2+\mathcal{L}_1}{2}, \tag{A4b}$$

$$\mathcal{R}(0,-1) = \tfrac{1}{2}(1+x^2-y^2)\lambda^{1/2} - x^2(\mathcal{L}_2-\mathcal{L}_1), \tag{A4c}$$

$$\mathcal{R}_{(1,-1)} = -\tfrac{1}{3}\lambda^{3/2} + (1+x^2)[\tfrac{1}{2}(1+x^2-y^2)\lambda^{1/2} - x^2(\mathcal{L}_2-\mathcal{L}_1)], \tag{A4d}$$

$$\mathcal{R}_{(-2,0)} = \frac{1}{y^2} - \frac{1}{(1-x)^2}, \quad \mathcal{R}^0_{(-1,0)} = 2\mathcal{L}_5, \tag{A4e}$$

$$\mathcal{R}_{(0,0)} = (1-x)^2 - y^2, \quad \mathcal{R}_{(1,0)} = \frac{(1-x)^4}{2} - \frac{y^4}{2}, \quad \mathcal{R}_{(2,0)} = \frac{(1-x)^6}{3} - \frac{y^6}{3}, \tag{A4f}$$

$$\mathcal{R}_{(-2,1)} = \frac{1}{(1-x^2)^2}\left(\frac{\lambda^{1/2}}{y^2} + \frac{1+x^2}{1-x^2}\,\frac{\mathcal{L}_2+\mathcal{L}_1}{2}\right), \quad \mathcal{R}_{(-1,1)} = \frac{1}{1-x^2}\,\frac{\mathcal{L}_2+\mathcal{L}_1}{2}, \tag{A4g}$$

$$\mathcal{R}_{(0,1)} = \frac{\mathcal{L}_2-\mathcal{L}_1}{2}, \quad \mathcal{R}_{(1,1)} = -\lambda^{1/2} + (1+x^2)\,\frac{\mathcal{L}_2-\mathcal{L}_1}{2}, \tag{A4h}$$

$$\mathcal{R}_{(2,1)}=-\frac{1}{2}y^2\lambda^{1/2}-\frac{3}{2}(1+x^2)\lambda^{1/2}+(1+4x^2+x^4)\times\frac{\mathcal{L}_2-\mathcal{L}_1}{2}, \tag{A4i}$$

$$\mathcal{R}_{(3,1)}=-\frac{1}{3}\lambda^{3/2}+\frac{3}{2}(1+x^2)(1+x^2-y^2)\lambda^{1/2}-(3+x^2)(1+3x^2)\lambda^{1/2}+(1+x^2)\times(1+8x^2+x^4)\frac{\mathcal{L}_2-\mathcal{L}_1}{2}, \tag{A4j}$$

$$\mathcal{R}_{(-2,2)}=\frac{1}{4x}\frac{\mathcal{L}_3}{(1-x)^4}-\frac{1}{4x}\frac{\mathcal{L}_4}{(1+x)^4}+\frac{1}{(1-x^2)^2}\times\left(\frac{1}{y^2}-\frac{1}{(1-x)^2}\right), \tag{A4k}$$

$$\mathcal{R}_{(-1,2)}=\frac{1}{4x}\frac{\mathcal{L}_3}{(1-x)^2}-\frac{1}{4x}\frac{\mathcal{L}_4}{(1+x)^2}, \tag{A4l}$$

$$\mathcal{R}_{(0,2)}=\frac{1}{4x}(\mathcal{L}_3-\mathcal{L}_4),$$

$$\mathcal{R}_{(1,2)}=\frac{(1-x)^2}{4x}\mathcal{L}_3-\frac{(1+x)^2}{4x}\mathcal{L}_4-\frac{1}{2x}\beta_-(2)\mathcal{L}_5, \tag{A4m}$$

$$\mathcal{R}_{(2,2)}=\frac{(1-x)^4}{4x}\mathcal{L}_3-\frac{(1+x)}{4x}\mathcal{L}_4-\frac{1}{2x}\beta_-(4)\mathcal{L}_5+[(1-x)^2-y^2], \tag{A4n}$$

$$\mathcal{R}_{(3,2)}=\frac{(1-x)^6}{4x}\mathcal{L}_3-\frac{(1+x)^6}{4x}\mathcal{L}_4-\frac{1}{2x}\beta_-(6)\mathcal{L}_5+3[(1-x)^2-y^2](1+x^2)-\frac{1}{2}\lambda, \tag{A4o}$$

$$\mathcal{R}_{(4,2)}=\frac{(1-x)^8}{4x}\mathcal{L}_3-\frac{(1+x)^8}{4x}\mathcal{L}_4-\frac{1}{2x}\beta_-(8)\mathcal{L}_5+[(1-x^2)-y^2]\left(\frac{1}{3}(1+x+x^2-y^2)^2+(6+17x^2+6x^4)\right)-2(1+x^2)\lambda. \tag{A4p}$$

3. Integrals of type $\mathcal{R}_{(n)}$

$$\mathcal{R}_{(-1)}=-\lambda^{1/2}-(1+x^2-y^2)\frac{\mathcal{L}_2-\mathcal{L}_1}{2}+\lambda^{1/2}\ln\left(\frac{\lambda^{1/2}}{x}\frac{\eta}{\epsilon^2}\right), \tag{A5a}$$

$$\mathcal{R}_{(0)}=\frac{1}{2}\ln\left(\frac{(1-x)^2-y^2}{(1+x)^2-y^2}\right)+\ln\left(\frac{\eta}{\epsilon_2}\right), \tag{A5b}$$

4. Integrals of type $\mathcal{S}_{(m,n)}$

$$\mathcal{S}_{(0,0)}=\lambda^{1/2}-x^2(\mathcal{L}_2-\mathcal{L}_1)-y^2\mathcal{L}_1, \tag{A6a}$$

$$\mathcal{S}_{(1,0)}=\frac{1}{4}(1+5x^2+y^2)\lambda^{1/2}-(2+x^2)x^2\frac{\mathcal{L}_2-\mathcal{L}_1}{2}-y^4\frac{\mathcal{L}_1}{2}, \tag{A6b}$$

$$\mathcal{S}_{(0,1)}=\mathcal{N}_0,\quad \mathcal{S}_{(1,1)}=(1+x^2)\mathcal{N}_0-\lambda^{1/2}\mathcal{L}_1+2(1-x^2)\mathcal{L}_5-[(1-x)^2-y^2], \tag{A6c}$$

$$\mathcal{S}_{(2,1)}=(1+4x^2+x^4)\mathcal{N}_0-\tfrac{1}{2}(3+3x^2+y^2)\lambda^{1/2}\mathcal{L}_1+3(1-x^4)\mathcal{L}_5-\tfrac{1}{4}[(1-x)^2-y^2][(1-x)^2+4+8x^2+y^2], \tag{A6d}$$

$$\mathcal{S}_{(0,2)}=-\frac{1}{2x}(\mathcal{N}_2-\mathcal{N}_3), \tag{A6e}$$

$$\mathcal{S}_{(1,2)}=-\frac{(1+x)^2}{2x}\mathcal{N}_2+\frac{(1-x)^2}{2x}\mathcal{N}_3+\mathcal{N}_1, \tag{A6f}$$

$$\mathcal{S}_{(2,2)}=-\frac{(1+x)^4}{2x}\mathcal{N}_2+\frac{(1-x)^4}{2x}\mathcal{N}_3+2(1+x^2)\mathcal{N}_1+\lambda^{1/2}-x^2(\mathcal{L}_2-\mathcal{L}_1)-y^2\mathcal{L}_1, \tag{A6g}$$

$$\mathcal{S}_{(3,2)}=-\frac{(1+x)^6}{2x}\mathcal{N}_2+\frac{(1-x)^6}{2x}\mathcal{N}_3+(3+x^2)\times(1+3x^2)\mathcal{N}_1+\frac{1}{4}(9+13x^2+y^2)\lambda^{1/2}-(6+5x^2)x^2\frac{\mathcal{L}_2-\mathcal{L}_1}{2}-y^2[4(1+x^2)+y^2]\frac{\mathcal{L}_1}{2}, \tag{A6h}$$

$$\mathcal{S}_{(0,3)}=\frac{1}{4x}\left\{\frac{2}{1-x}+\frac{1}{1-x}\mathcal{L}_3-\frac{1}{1+x}\mathcal{L}_4-\frac{\beta(0)}{x}\mathcal{L}_1+\frac{\beta_+(0)}{x}\mathcal{L}_6\right\}, \tag{A6i}$$

$$\mathcal{S}_{(1,3)}=\frac{1}{4x}\left\{2(1-x)+(1-x)\mathcal{L}_3-(1+x)^3\mathcal{L}_4-\frac{\beta(2)}{x}\mathcal{L}_1+\frac{\beta_+(2)}{x}\mathcal{L}_6\right\}, \tag{A6j}$$

$$\mathcal{S}_{(2,3)}=\frac{1}{4x}\Bigg\{2(1-x)^3+(1-x)^3\mathcal{L}_3-(1+x)^3\mathcal{L}_4 - \frac{\beta(4)}{x}\mathcal{L}_1+\frac{\beta_+(4)}{x}\mathcal{L}_6+4x\mathcal{N}_0\Bigg\}, \tag{A6k}$$

$$\mathcal{S}_{(3,3)}=\frac{1}{4x}\Bigg\{2(1-x)^5+(1-x)^5\mathcal{L}_3-(1+x)^5\mathcal{L}_4 - \frac{\beta(6)}{x}\mathcal{L}_1+\frac{\beta_+(6)}{x}\mathcal{L}_6+12x(1+x^2)\mathcal{N}_0 +8x(1-x^2)\mathcal{L}_5-4x\lambda^{1/2}\mathcal{L}_1 -4x[(1-x)^2-y^2]\Bigg\}, \tag{A6l}$$

$$\mathcal{S}_{(4,3)}=\frac{1}{4x}\Bigg\{2(1-x)^7+(1-x)^7\mathcal{L}_3-(1+x)^7\mathcal{L}_4 - \frac{\beta(8)}{x}\mathcal{L}_1+\frac{\beta_+(8)}{x}\mathcal{L}_6+24x(1+3x^2+x^4)\mathcal{N}_0 +28x(1-x^4)\mathcal{L}_5-2x(7+7x^2+y^2)\lambda^{1/2}\mathcal{L}_1 -2x[(1-x)^2-y^2](7+9x^2)+x\lambda\Bigg\}. \tag{A6m}$$

5. Integrals of type $\mathcal{S}_{(n)}$

$$\mathcal{S}_{(0)}=-\frac{\mathcal{L}_1^2}{2}+\mathcal{L}_1\ln\left(\frac{\lambda^{1/2}}{x}\frac{\eta}{\epsilon_2}\right)+(\mathcal{L}_2-\mathcal{L}_1)\ln y+\mathrm{Li}_2(\eta x) -\mathrm{Li}_2\left(\frac{x}{\eta}\right)-2\,\mathrm{Li}_2\left(\frac{(\eta^2-1)x}{\eta-x}\right), \tag{A7a}$$

$$\mathcal{S}_{(1)}=\frac{1}{\lambda^{1/2}}\Bigg\{-\frac{\mathcal{L}_1^2}{2}+\mathcal{L}_1\ln\left(\frac{\lambda^{1/2}}{x}\frac{1}{\epsilon_2}\right)+2\,\mathrm{Li}_2\left(-\frac{1}{\eta}\right) -2\,\mathrm{Li}_2\left(-\frac{1-\eta x}{\eta-x}\right)\Bigg\}. \tag{A7b}$$

Of all the many integrals listed in Secs. A 2–A 5 the total rate calculation done before in [3–8] requires only the five basic integrals $\mathcal{R}_{(-2,-1)}$, $\mathcal{R}_{(-1,-1)}$, $\mathcal{R}_{(0,-1)}$, $\mathcal{S}_{(0,0)}$, and $\mathcal{S}_{(1,0)}$ compared to the 33 basic integrals that are needed for the full calculation. This may serve as a measure of the additional labor that is incurred when one calculates the complete set of structure functions as is done in this paper.

APPENDIX B: COEFFICIENT FUNCTIONS $\rho_{(n)}$, $\rho_{(m,n)}$, $\sigma_{(n)}$, and $\sigma_{(m,n)}$

In this appendix we list the values of the various coefficient functions $\rho_{(n),i}$, $\rho_{(m,n),i}$, $\sigma_{(n),i}$, and $\sigma_{(m,n),i}$ ($i=U+L$, U^P+L^P, U, U^P, L, L^P, F, F^P, S, S^P, I^P, and A^P) that multiply the basic set of integrals listed in Appendix A as spelled out in the rate expression Eq. (60). The coefficient functions involve polynomials in x^2 and y^2 which we sort by increasing powers of y^2. For reasons of conciseness we drop the suffix y denoting the particular type of structure function in the following listing. The contributions are collected in terms of powers of y^2.

1. Total rate $i=U+L$

$$\rho_{(-2,-1)}=-\frac{y^2(1-x^2)((1+2x^2)+y^2)}{x^2}, \tag{B1a}$$

$$\rho_{(-1,-1)}=\frac{(1-x^2)(1+2x^2)+(4-3x^2)y^2+3y^4}{x^2} \tag{B1b}$$

$$\rho_{(0,-1)}=-\frac{(3-2x^2)+3y^2}{x^2}, \tag{B1c}$$

$$\sigma_{(0,0)}=-2\frac{y^2((1+2x^2)+y^2)}{x^2}, \tag{B1d}$$

$$\sigma_{(1,0)}=2\frac{(1+2x^2)+y^2}{x^2}. \tag{B1e}$$

2. Polarized total rate $i=U^P+L^P$

$$\rho_{(-2,0)}=-\frac{y^2(1-x^2)^2[(1-2x^2)-y^2]}{x^2}, \tag{B2a}$$

$$\rho_{(-1,0)}=\frac{(1-4x^2+5x^4-2x^6)+(5-4x^2-5x^4)y^2-2(3-x^2)y^4}{x^2}, \tag{B2b}$$

$$\rho_{(0,0)}=\frac{2(1-x^2-6x^4)-3y^2+y^4}{x^2}, \tag{B2c}$$

$$\rho_{(1,0)}=-\frac{(7-6x^2)-7y^2}{x^2}, \tag{B2d}$$

$$\rho_{(-1)}=8\frac{\sqrt{\lambda}[(1-2x^2)-y^2]}{x^2}, \tag{B2e}$$

$$\rho_{(0)} = -8\,\frac{\lambda[(1-2x^2)-y^2]}{x^2}, \tag{B2f}$$

$$\sigma_{(0,0)} = -4\,\frac{\sqrt{\lambda}[(1-2x^2)-y^2]}{x^2}, \tag{B2g}$$

$$\sigma_{(0,1)} = -2\,\frac{4x^2(1-2x^2)(1-x^2)+(7-5x^2-6x^4)y^2-(9+x^2)y^4+2y^6}{x^2}, \tag{B2h}$$

$$\sigma_{(1,1)} = 2\,\frac{(3-x^2+6x^4)-(2-x^2)y^2-y^4}{x^2}, \tag{B2i}$$

$$\sigma_{(2,1)} = 2\,\frac{(1-2x^2)-y^2}{x^2}, \tag{B2j}$$

$$\sigma_{(0)} = 4\,\frac{\sqrt{\lambda}(1-x^2+y^2)[(1-2x^2)-y^2]}{x^2}, \tag{B2k}$$

$$\sigma_{(1)} = 4\,\frac{\lambda(1-x^2+y^2)[(1-2x^2)-y^2]}{x^2}. \tag{B2l}$$

3. Longitudinal rate $i=L$

$$\rho_{(-2,1)} = -\,\frac{y^2(1+y^2)(1-x^2)^3}{x^2}, \tag{B3a}$$

$$\rho_{(-1,1)} = \frac{(1-x^2)[(1-x^2)^2+(6+x^2-3x^4)y^2+(5+3x^2)y^4]}{x^2}, \tag{B3b}$$

$$\rho_{(0,1)} = -\,\frac{(5-2x^2-7x^4+4x^6)+(12-33x^2+x^4)y^2+(7+x^2)y^4}{x^2}, \tag{B3c}$$

$$\rho_{(1,1)} = \frac{(7-31x^2+4x^4)+(10+x^2)y^2+3y^4}{x^2}, \tag{B3d}$$

$$\rho_{(2,1)} = -3\,\frac{1+y^2}{x^2}, \tag{B3e}$$

$$\sigma_{(0,2)} = -2\,\frac{y^2[(1+10x^2-11x^4)+(1+x^2)y^2y^2]}{x^2}, \tag{B3f}$$

$$\sigma_{(1,2)} = 2\,\frac{(1+10x^2-11x^4)+(3-4x^2+x^4)y^2+2(1+x^2)y^4}{x^2}, \tag{B3g}$$

$$\sigma_{(2,2)} = -2\,\frac{2(1-3x^2)+(3+2x^2)y^2+y^4}{x^2}, \tag{B3h}$$

$$\sigma_{(3,2)} = 2\,\frac{1+y^2}{x^2}. \tag{B3i}$$

4. Polarized longitudinal rate $i=L^P$

$$\rho_{(-2,2)}=-\frac{y^2(1-y^2)(1-x^2)^4}{x^2}, \tag{B4a}$$

$$\rho_{(-1,2)}=\frac{(1-x^2)^2[(1-x^2)^2+(7-2x^2+3x^4)y^2-4(2+x^2)y^4]}{x^2}, \tag{B4b}$$

$$\rho_{(0,2)}=2\frac{2x^2(3-x^2)(1-x^2)^2-(7-5x^4+6x^6)y^2+(7-18x^2+3x^4)y^4}{x^2}, \tag{B4c}$$

$$\rho_{(1,2)}=-2\frac{(5+10x^2+13x^4-4x^6)-(9+48x^2+11x^4)y^2+2(2+x^2)y^4}{x^2}, \tag{B4d}$$

$$\rho_{(2,2)}=\frac{(16-20x^2-4x^4)-(17+20x^2)y^2+y^4}{x^2}, \tag{B4e}$$

$$\rho_{(3,2)}=-7\frac{1-y^2}{x^2}, \tag{B4f}$$

$$\sigma_{(-1)}=8\frac{\sqrt{\lambda}(1-y^2)}{x^2}, \tag{B4g}$$

$$\sigma_{(0)}=-8\frac{\lambda(1-y^2)}{x^2}, \tag{B4h}$$

$$\sigma_{(0,0)}=-4\frac{\sqrt{\lambda}(1-y^2)}{x^2}, \tag{B4i}$$

$$\sigma_{(0,3)}=-2\frac{(1-x^2)[4x^2(1-x^2)^2+(7-10x^2+7x^4-4x^6)y^2]}{x^2}+2\frac{(1-x^2)[(9+8x^2-5x^4)y^4-2(1-x^2)y^6]}{x^2}, \tag{B4j}$$

$$\sigma_{(1,3)}=2\frac{(3-5x^2+17x^4-15x^6)+(12-9x^2+18x^4+11x^6)y^2}{x^2}-2\frac{(19+14x^2+11x^4)y^4-4(1+x^2)y^6}{x^2}, \tag{B4k}$$

$$\sigma_{(2,3)}=-2\frac{(5-14x^2-7x^4)+(4+21x^2+11x^4)y^2-(11+7x^2)y^4+2y^6}{x^2}, \tag{B4l}$$

$$\sigma_{(3,3)}=2\frac{(1+3x^2)+5x^2y^2-y^4}{x^2}, \tag{B4m}$$

$$\sigma_{(4,3)}=2\frac{1-y^2}{x^2}, \tag{B4n}$$

$$\sigma_{(0)}=-4\frac{\sqrt{\lambda}(1-y^2)(1-x^2+y^2)}{x^2}, \tag{B4o}$$

$$\sigma_{(1)}=4\frac{\lambda(1-y^2)(1-x^2+y^2)}{x^2}. \tag{B4p}$$

5. Unpolarized transverse rate $i=U$

$$\rho_{(-2,1)}=-2y^2(1-x^2)^3, \tag{B5a}$$

$$\rho_{(-1,1)}=2(1-x^2[(1-x^2)^2-(1-5x^2)y^2-2y^4], \tag{B5b}$$

$$\rho_{(0,1)}=2[(1-6x^2+5x^4)-3(5-x^3)y^2-2y^4], \tag{B5c}$$

$$\rho_{(1,1)}=2[(17-5x^2)+y^2], \tag{B5d}$$

$$\rho_{(2,1)}=2, \tag{B5e}$$

$$\sigma_{(0,2)}=4y[(5-4x^2-x^4)+2u^2], \tag{A5f}$$

$$\sigma_{(1,2)}=-4[(5-4x^2-x^4)-2(2+x^2)y^2], \tag{B5g}$$

$$\sigma_{(2,2)}=-4[(6+2x^2)+y^2], \tag{B5h}$$

$$\sigma_{(3,2)}=4. \tag{B5i}$$

6. Polarized unpolarized-transverse rate $i=U^P$

$$\rho_{(-2,2)}=2y^2(1-x^2)^4, \tag{B6a}$$

$$\rho_{(-1,2)}=-2(1-x^2)^2[(1-x^2)^2+2(1+3x^2)y^2-2y^4], \tag{B6b}$$

$$\rho_{(0,2)}=-4[(1-x^2)^2(3+x^2)-2(1+3x^4)y^2-2(5-x^2)y^4], \tag{B6c}$$

$$\rho_{(1,2)}=4[(9+10x^2+5x^4)-(27+5x^2)y^2+y^4], \tag{B6d}$$

$$\rho_{(2,2)}=2[10(1-x^2)+3y^2], \tag{B6e}$$

$$\rho_{(3,2)}=6, \tag{B6f}$$

$$\rho(-1)=-16\sqrt{\lambda}, \tag{B6g}$$

$$\sigma_{(0)}=16\lambda, \tag{B6h}$$

$$\sigma_{(0,0)}=8\sqrt{\lambda}, \tag{B6i}$$

$$\sigma_{(0,3)}=4(1-x^2)[4x^2(1-x^2)^2+(1+4x^2-5x^4)y^2-2(4-x^2)y^4], \tag{B6j}$$

$$\sigma_{(1,3)}=4[(1-x^4)(3-11x^2)+(9-22x^2-11x^4)y^2-2(1-2x^2)y^4], \tag{B6k}$$

$$\sigma_{(2,3)}=-4[(13+11x^4)-(15+7x^2)y^2+2y^4], \tag{B6l}$$

$$\sigma_{(3,3)}=-4[(1-5x^2)+y^2], \tag{B6m}$$

$$\sigma_{(4,3)}=-4, \tag{B6n}$$

$$\sigma_{(0)}=8\sqrt{\lambda}(1-x^2+y^2), \tag{B6o}$$

$$\sigma_{(1)}=-8\lambda(1-x^2+y^2). \tag{B6p}$$

7. Scalar rate $i=S$

$$\rho_{(-2,-1)}2=-\frac{y^2(1+y^2)(1-x^2)}{x^2}, \tag{B7a}$$

$$\rho_{(-1,-1)}=\frac{(1+y^2)[(1-x^2)+3y^2]}{x^2}, \tag{B7b}$$

$$\rho_{(0,-1)}=-3\frac{(1+y^2)}{x^2}, \tag{B7c}$$

$$\sigma_{(0,0)}=-2\frac{y^2(1+y^2)}{x^2}, \tag{B7d}$$

$$\sigma_{(1,0)}=2\frac{(1+y^2)}{x^2}. \tag{B7e}$$

8. Polarized scalar rate $i=S^P$

$$\rho_{(-2,0)}=-\frac{y^2(1-y^2)(1-x^2)^2}{x^2}, \tag{B8a}$$

$$\rho_{(-1,0)}=\frac{(1-y^2)[(1-x^2)^2+2(3-x^2)y^2]}{x^2}, \tag{B8b}$$

$$\rho_{(0,0)}=\frac{(1-y^2)[2(1+5x^2)-y^2]}{x^2}, \tag{B8c}$$

$$\rho_{(1,0)}=-7\frac{1-y^2)}{x^2}, \tag{B8d}$$

$$\rho_{(-1)}=8\frac{\sqrt{\lambda}(1-y^2)}{x^2}, \tag{B8e}$$

$$\rho_{(0)}=-8\frac{\lambda(1-y^2)}{x^2}, \tag{B8f}$$

$$\sigma_{(0,0)}=-4\frac{\sqrt{\lambda}(1-y^2)}{x^2}, \tag{B8g}$$

$$\sigma_{(0,1)}=-2\frac{(1-y^2)[4x^2(1-x^2)+(7+5x^2)y^2-2y^4]}{x^2}, \tag{B8h}$$

$$\sigma_{(1,1)}=2\frac{(1-y^2)[3(1-x^2)+y^2]}{x^2}, \tag{B8i}$$

$$\sigma_{(2,1)}=2\frac{(1-y^2)}{x^2}, \tag{B8j}$$

$$\sigma_{(0)} = -4\,\frac{\sqrt{\lambda}(1-y^2)[(1-x^2)+y^2]}{x^2}, \tag{B8k}$$

$$\sigma_{(1)} = 4\,\frac{\lambda(1-y^2)[(1-x^2)+y^2]}{x^2}. \tag{B8l}$$

9. Forward-backward-asymmetric rate $i=F$

$$\rho_{(-2,0)} = -2y^2(1-x^2)^2, \tag{B9a}$$

$$\rho_{(-1,0)} = 2[(1-x^2)^2+4x^2y^2], \tag{B9b}$$

$$\rho_{(0,0)} = 2[4(2+x^2)-7y^2], \tag{B9c}$$

$$\rho_{(1,0)} = -2, \tag{B9d}$$

$$\rho_{(-1)} = 16\sqrt{\lambda}, \tag{B9e}$$

$$\rho_{(0)} = -16\lambda, \tag{B9f}$$

$$\sigma_{(0,0)} = -8\sqrt{\lambda}, \tag{B9g}$$

$$\sigma_{(0,1)} = -4[4x^2(1-x^2)+(1+5x^2)y^2-2y^4], \tag{B9h}$$

$$\sigma_{(1,1)} = -4[3(1+x^2)-y^2], \tag{B9i}$$

$$\sigma_{(2,1)} = 4, \tag{B9j}$$

$$\sigma_{(0)} = -8\sqrt{\lambda}[(1-x^2)+y^2], \tag{B9k}$$

$$\sigma_{(1)} = 8\lambda[(1-x^2)+y^2], \tag{B9l}$$

10. Polarized forward-backward-asymmetric rate $i=F^P$

$$\rho_{(-2,1)} = 2y^2(1-x^2)^3, \tag{B10a}$$

$$\rho_{(-1,1)} = -2(1-x^2)[(1-x^2)^2-(1-5x^2)y^2], \tag{B10b}$$

$$\rho_{(0,1)} = -2[(1-6x^2+5x^4)-(11+x^2)y^2], \tag{B10c}$$

$$\rho_{(1,1)} = -2[(11+x^2)+5y^2], \tag{B10d}$$

$$\rho_{(2,1)} = 10, \tag{B10e}$$

$$\rho_{(0,2)} = -4y^2(1-x^2)(5+x^2), \tag{B10f}$$

$$\sigma_{(1,2)} = 4[(1-x^2)(5+x^2)-2x^2y^2], \tag{B10g}$$

$$\sigma_{(2,2)} = 4(2x^2+y^2), \tag{B10h}$$

$$\sigma_{(3,2)} = -4. \tag{B10i}$$

11. Polarized longitudinal-transverse-interference rate $i=I^P$

$$\rho_{(-2,2)} = \frac{\sqrt{2}}{2}\,\frac{y^2(1-x^2)^4}{x}, \tag{B11a}$$

$$\rho_{(-1,2)} = -\frac{\sqrt{2}}{2}\,\frac{(1-x^2)^2[(1-x^2)^2+(3+5x^2)y^2+2y^4]}{x}, \tag{B11b}$$

$$\rho_{(0,2)} = -\frac{\sqrt{2}}{2}\,\frac{(1-x^2)^2(5+3x^2)-(25-38x^2+29x^4)y^2+8(1+x^2)y^4}{x}, \tag{B11c}$$

$$\rho_{(1,2)} = \frac{\sqrt{2}}{2}\,\frac{(1+50x^2-3x^4)-(21+23x^2)y^2+10y^4}{x}, \tag{B11d}$$

$$\rho_{(2,2)} = \frac{\sqrt{2}}{2}\,\frac{(5+7x^2)-2y^2}{x}, \tag{B11e}$$

$$\rho_{(-1)} = -4\sqrt{2}\,\frac{\sqrt{\lambda}}{x}, \tag{B11f}$$

$$\rho_{(0)} = 4\sqrt{2}\,\frac{\lambda}{x}, \tag{B11g}$$

$$\sigma_{(0,0)} = 2\sqrt{2}\,\frac{\sqrt{\lambda}}{x}, \tag{B11h}$$

$$\sigma_{(0,3)} = \sqrt{2}\,\frac{(1-x^2)[4x^2(1-x^2)^2-(1-9x^2+8x^4)y^2+2(1+2x^2)y^4]}{x}, \tag{B11i}$$

$$\sigma_{(1,3)}=\sqrt{2}\,\frac{(5-18x^2+5x^4+8x^6)-2(5+x^2+8x^4)y^2+2(1+4x^2)y^4}{x}, \tag{B11j}$$

$$\sigma_{(2,3)}=-\sqrt{2}\,\frac{4(1+3x^2+x^4)-(11+8x^2)+4y^4}{x}, \tag{B11k}$$

$$\sigma_{(3,3)}=-\sqrt{2}\,\frac{1}{x}, \tag{B11l}$$

$$\sigma_{(0)}=2\sqrt{2}\,\frac{\sqrt{\lambda}[(1-x^2)+y^2]}{x}, \tag{B11m}$$

$$\sigma_{(1)}=-2\sqrt{2}\,\frac{\lambda[(1-x^2)+y^2]}{x}. \tag{B11n}$$

12. Polarized parity-asymmetric rate $i=A^P$

$$\rho_{(-2,1)}=\frac{\sqrt{2}}{2}\,\frac{y^2(1-x^2)^3}{x}, \tag{B12a}$$

$$\rho_{(-1,1)}=-\frac{\sqrt{2}}{2}\,\frac{(1-x^2)[(1-x^2)^2+4y^2]}{x}, \tag{B12b}$$

$$\rho_{(0,1)}=\frac{\sqrt{2}}{2}\,\frac{4(1-x^2)+(3-7x^2)y^2}{x}, \tag{B12c}$$

$$\rho_{(1,1)}=-\frac{\sqrt{2}}{2}\,\frac{3-7x^2}{x}, \tag{B12d}$$

$$\sigma_{(0,2)}=\sqrt{2}\,\frac{y^2(1-x^2)(1+2x^2)}{x}, \tag{B12e}$$

$$\sigma_{(1,2)}=-\sqrt{2}\,\frac{(1-x^2)(1+2x^2)+(1-2x^2)y^2}{x}, \tag{B12f}$$

$$\sigma_{(2,2)}=\sqrt{2}\,\frac{1-2x^2}{x}. \tag{B12g}$$

APPENDIX C: LOOP INTEGRALS

In this appendix we list the $m_b\neq 0$ one-loop amplitude corrections to the process $t\to b+W^+$. They are determined from the vertex correction Fig. 1(b) and the appropriate wave function renormalization constants Z_2. We present our results in terms of the three vector current amplitudes F_i^V $(i=1,2,3)$ and the three axial vector current amplitudes F_i^A $(i=1,2,3)$ defined in Eq. (25a) in Sec. V. Using the abbreviations in Eq. (64) with $q^2=m_W^2$, one has

$$\begin{aligned}F_1^V=1+\frac{\alpha_s}{4\pi}C_F\Bigg\{&-\frac{m_t^2+m_b^2-q^2}{m_t^2\sqrt{\lambda}}\Bigg[2\,\mathrm{Li}_2(1-w_1^2)\\&-2\,\mathrm{Li}_2\left(1-\frac{w_1}{w_\mu}\right)+\frac{1}{2}\ln\left(\frac{\Lambda^4}{m_b^2m_t^2}\right)\ln(w_1w_\mu)\\&+\ln\left(\frac{w_1^3}{w_\mu}\right)\ln\left(\frac{w_\mu(1-w_1^2)}{w_\mu-w_1}\right)\Bigg]-\ln\left(\frac{\Lambda^4}{m_b^2m_t^2}\right)\\&-\frac{m_t^2-m_b^2}{2q^2}\ln\left(\frac{m_b^2}{m_t^2}\right)-4+\ln(w_1w_\mu)\\&\times\left(\frac{m_t^2\sqrt{\lambda}}{2q^2}-\frac{(m_t+m_b)^2-q^2}{m_t^2\sqrt{\lambda}}\right)\Bigg\},\end{aligned} \tag{C1}$$

$$\begin{aligned}F_2^V=\frac{\alpha_s}{4\pi}C_F\frac{m_t-m_b}{q^2}\Bigg\{&2-\Bigg(\frac{m_t+2m_b}{m_t-m_b}\\&-\frac{m_t^2-m_b^2}{q^2}\Bigg)\ln\left(\frac{m_b^2}{m_t^2}\right)-\Bigg(\frac{m_t^2\sqrt{\lambda}}{q^2}-\frac{m_b}{m_t-m_b}\\&\times\frac{q^2+(m_t-m_b)(3m_t+m_b)}{m_t^2\sqrt{\lambda}}\Bigg)\ln(w_1w_\mu)\Bigg\},\end{aligned} \tag{C2}$$

$$F_3^V=F_3^V(m_t,m_b)=F_2^V(m_b,m_t). \tag{C3}$$

As before the IR singularity is regularized by a small gluon mass m_g. The axial vector amplitudes F_i^A can be obtained from the vector amplitudes by the replacement $m_t\to -m_t$, i.e., one has $F_i^A(m_t)=F_i^V(-m_t)$ $(i=1,2,3)$. Our one-loop amplitudes are linearly related to the one-loop amplitudes given in [34]. The two sets of one-loop amplitudes agree with each other after correcting for a typo in [34] mentioned in Sec. V.

[1] CDF Collaboration, T. Affolder *et al.*, Phys. Rev. Lett. **84**, 216 (2000).
[2] S. Willenbrock, Rev. Mod. Phys. **72**, 1141 (2000); M. Narain (private communication).
[3] A. Denner and T. Sack, Nucl. Phys. **B358**, 46 (1991).
[4] J. Liu and Y.-P. Yao, Int. J. Mod. Phys. A **6**, 4925 (1991).
[5] A. Czarnecki, Phys. Lett. B **252**, 467 (1990).
[6] C. S. Li, R. J. Oakes, and T. C. Yuan, Phys. Rev. D **43**, 3759 (1991).
[7] M. Jezabek and J. H. Kühn, Nucl. Phys. **B314**, 1 (1989).
[8] A. Ghinculov and Y. P. Yao, Mod. Phys. Lett. A **15**, 925 (2000).
[9] G. Mahlon and S. Parke, Phys. Rev. D **55**, 7249 (1997).
[10] J. H. Kühn, A. Reiter, and P. Zerwas, Nucl. Phys. **B272**, 560 (1986).
[11] M. Anselmino, P. Kroll, and B. Pire, Phys. Lett. **167B**, 113 (1986).
[12] J. G. Körner, A. Pilaftsis, and M. M. Tung, Z. Phys. C **63**, 575 (1994).
[13] S. Groote, J. G. Körner, and M. M. Tung, Z. Phys. C **74**, 615 (1997).
[14] S. Groote and J. G. Körner, Z. Phys. C **74**, 255 (1996).
[15] S. Groote, J. G. Körner, and M. M. Tung, Z. Phys. C **70**, 281 (1996).
[16] M. Fischer, S. Groote, J. G. Körner, B. Lampe, and M. C. Mauser, Phys. Lett. B **451**, 406 (1999).
[17] S. Parke and Y. Shadmi, Phys. Lett. B **387**, 199 (1996).
[18] M. M. Tung, J. Bernabeu, and J. Penarrocha, Phys. Lett. B **418**, 181 (1998).
[19] S. Groote, J. G. Körner, and A. J. Leyva, Phys. Lett. B **418**, 192 (1998).
[20] A. Brandenburg, M. Flesch, and P. Uwer, Phys. Rev. D **59**, 014001 (1999).
[21] G. Mahlon and S. Parke, Phys. Rev. D **53**, 4886 (1996); Phys. Lett. B **411**, 173 (1997).
[22] A. Czarnecki, M. Jezabek, and J. H. Kühn, Nucl. Phys. **B351**, 70 (1991); A. Czarnecki, M. Jezabek, J. G. Körner, and J. H. Kühn, Phys. Rev. Lett. **73**, 384 (1994); A. Czarnecki and M. Jezabek, Nucl. Phys. **B427**, 3 (1994).
[23] M. Fischer, S. Groote, J. G. Körner, and M. C. Mauser, Phys. Rev. D **63**, 031501R (2001).
[24] A. Czarnecki and S. Davidson, Phys. Rev. D **47**, 3063 (1993); **48**, 4183 (1993).
[25] H. S. Do, S. Groote, J. G. Körner, and M. C. Mauser (unpublished).
[26] M. Jezabek and J. H. Kühn, Phys. Rev. D **48**, 1910 (1993); **49**, 4970(E) (1994).
[27] B. Lampe, Nucl. Phys. **B458**, 23 (1996).
[28] B. Lampe, Nucl. Phys. **B454**, 506 (1995).
[29] B. Lampe, hep-ph/9801346.
[30] P. Bialas, J. G. Körner, M. Krämer, and K. Zalewski, Z. Phys. C **57**, 115 (1993).
[31] A. A. Penin and A. A. Pivovarov, Nucl. Phys. **B549**, 217 (1999); Phys. Lett. B **443**, 264 (1998).
[32] S. Groote, J. G. Körner, and M. M. Tung, Z. Phys. C **74**, 615 (1996); S. Groote, J. G. Körner, and J. A. Leyva, Phys. Lett. B **418**, 192 (1998).
[33] K. Schilcher, M. D. Tran, and N. F. Nasrallah, Nucl. Phys. **B181**, 91 (1981); **B187**, 594(E) (1981).
[34] G. J. Gounaris and J. E. Paschalis, Nucl. Phys. **B222**, 473 (1983).
[35] K. Fujikawa and A. Yamada, Phys. Rev. D **49**, 5890 (1994).
[36] P. Cho and M. Misiak, Phys. Rev. D **49**, 5894 (1994).
[37] B. Grzadkowski and J. Pliszka, Phys. Rev. D **63**, 115010 (2001).
[38] M. Fischer, S. Groote, J. G. Körner, and M. C. Mauser, Phys. Lett. B **480**, 265 (2000).
[39] R. Aleksan, M. Zito, A. Le Youanc, L. Oliver, O. Pene, and J. C. Raynal, Phys. Rev. D **62**, 093017 (2000).
[40] K. G. Chetyrkin, R. Harlander, T. Seidensticker, and M. Steinhauser, Phys. Rev. D **60**, 114015 (1999).
[41] G. Eilam, R. R. Mendel, R. Migneron, and A. Soni, Phys. Rev. Lett. **66**, 3105 (1991).
[42] G. Grunberg, Y. J. Ng, and S.-S. H. Tye, Phys. Rev. D **21**, 62 (1980).